Weierstraß-Institut
für Angewandte Analysis und Stochastik

Leibniz-Institut im Forschungsverbund Berlin e. V.

Preprint ISSN 2198-5855

A model framework for ion channels with selectivity filters based on continuum non-equilibrium thermodynamics

Christine Keller, Jürgen Fuhrmann, Manuel Landstorfer, Barbara Wagner

submitted: December 20, 2023

Weierstrass Institute
Mohrenstr. 39
10117 Berlin
Germany
E-Mail: christine.keller@wias-berlin.de
juergen.fuhrmann@wias-berlin.de
manuel.landstorfer@wias-berlin.de
barbara.wagner@wias-berlin.de

No. 3072
Berlin 2023

2020 *Mathematics Subject Classification.* 65Z05,92C05,92C40.

Key words and phrases. Ion channels, selectivity filter, continuum modeling, non-equilibrium thermodynamics.

C.K. gratefully acknowledges the financial support by the DFG under Germany's Excellence Strategy – MATH$^+$: The Berlin Mathematics Research Center (EXC-2046/1 – project ID: 390685689) via the project AA1-14.

Edited by
Weierstraß-Institut für Angewandte Analysis und Stochastik (WIAS)
Leibniz-Institut im Forschungsverbund Berlin e. V.
Mohrenstraße 39
10117 Berlin
Germany

Fax: +49 30 20372-303
E-Mail: preprint@wias-berlin.de
World Wide Web: http://www.wias-berlin.de/

A model framework for ion channels with selectivity filters based on continuum non-equilibrium thermodynamics

Christine Keller, Jürgen Fuhrmann, Manuel Landstorfer, Barbara Wagner

Abstract

A mathematical model framework to describe ion transport in nanopores is presented. The model is based on non-equilibrium thermodynamics and considers finite size effects, solvation phenomena as well as the electrical charges of membrane surfaces and channel proteins. Particular emphasis is placed on the consistent modelling of the selectivity filter in the pore. It is treated as an embedded domain in which the constituents can change their chemical properties. The diffusion process through the filter is governed by an independent diffusion coefficient and at the interfaces, de- and resolvation reactions are introduced as Neumann interface conditions. The evolution of the molar densities is described by drift-diffusion equations, where the fluxes depend on the gradient of the chemical potentials and the electric force. The chemical potentials depend on the molar fractions and on the pressure in the electrolyte and accounts for solvation effects. The framework allows the calculation of current-voltage relations for a variety of channel properties and ion concentrations. We compare our model framework to experimental results for calcium-selective ion channels and show the general validity of our approach. Our parameter studies show that calcium and sodium currents are proportional to the surface charge in the selectivity filter and to the diffusion coefficients of the ions. Moreover, they show that the negative charges inside the pore have a decisive influence on the selectivity of divalent over monovalent ions.

1 Introduction

The intricate and fundamental processes governing cellular functions are orchestrated by a myriad of biological ion channels that regulate the movement of ions across cell membranes. Among these channels, calcium ion channels hold a prominent position due to their vital role in various physiological functions [9,44]. Understanding the complex mechanisms underlying calcium ion channels is of great importance, as they play a crucial role in cellular signaling, muscle contraction, neurotransmitter release, gene expression, and a myriad of other cellular processes [9,10,20,44]. Traditional experimental techniques, such as electrophysiology and X-ray crystallography, have significantly contributed to our understanding of ion channels [14,54]. However, studying ion channels using traditional experimental techniques is a complex and challenging task.

As a result, the development of advanced modeling and simulation techniques has become essential in unravelling the mysteries of ion channels and providing deeper insights into their structure-function relationships and underlying mechanisms. This paper aims to explore the necessity of modeling and simulating biological ion channels, with a specific focus on Ca^{2+} ion channels, to bridge the gap between experimental observations and theoretical predictions. Computational modeling offers a powerful approach to complement experimental studies by providing in-depth insights into the behavior of ion channels at the molecular level. Molecular dynamics (MD) simulations, for example, can offer a very detailed description of the problem by resolving the structure of the ion channel protein at the atomic

DOI 10.20347/WIAS.PREPRINT.3072 Berlin 2023

level. This allows the study of individual ion channels in a controlled environment, capturing their conformational dynamics and interactions with ions and other molecules [21, 31]. MD simulations could, for example, contribute to a better understanding of the selectivity mechanisms within ion channels, especially in KcsA channels [13, 46, 47].

Understanding the molecular mechanisms of Ca^{2+} ion channels is not merely an academic pursuit; it holds significant implications for human health and disease. Dysregulation of these channels has been linked to a wide range of pathologies, including cardiac arrhythmias, neurodegenerative disorders, and cancer [9, 30, 44, 52]. By gaining a comprehensive understanding of Ca^{2+} ion channels through modeling and simulation, researchers can identify potential therapeutic targets for drug development and design more efficient and targeted interventions.

However, the molecular description is often computationally intensive, which results, for instance, in a limitation of the simulated time span. This on the other hand can lead to an incomplete depiction of experimental observations, which often span several seconds [2, 3]. A formulation of the problem on a coarse-grained macroscopic level can address this issue. Most such continuum models are based on Poisson-Nernst-Planck (PNP) theory, which has been successfully used to simulate semiconductor devices [29, 44, 48] and can be derived by averaging a Poisson-Langevin model [49]. Although not every atomistic detail is resolved, the PNP theory can make predictions about current-voltage (IV) relations and capture high variations in ion concentration, e.g. Ca^{2+} concentrations that range from 10^{-8} to $10^{-6}\,\mathrm{mol\,L^{-1}}$. However, several challenges persist, such as accurately representing ion-ion and ion-protein interactions, capturing solvent effects, and developing reliable force fields for membrane proteins. Great efforts have been made to overcome these problems and the Poisson-Nernst-Planck-Bikerman (PNPB) theory has been developed. Modified chemical potential functions with steric effects were formulated to account for finite size effects and to include water molecules [41]. For this purpose, entropies are often derived based on thermodynamic principles, such as density functional theory (DFT) [25, 27] or mean spherical approximation (MSA) [4, 41, 45]. An alternative approach is to derive a continuum formulation directly from a stochastic formulation such as hopping models [8]. As computational techniques continue to evolve, the integration of multi-scale simulations and machine learning approaches holds the promise of unraveling even more complex behaviors of Ca^{2+} ion channels. For example, MD simulations can be used to find stable ion configurations and calculate the channel geometry which is then used to solve the continuum model [32].

In this work, we present a continuum framework for ion channels in a liquid electrolyte environment based on non-equilibrium thermodynamics [12]. It provides a consistent coupling of diffusion and mechanics, so that the conservation of mass is fulfilled for the whole system. It couples of the momentum balance to the Nernst-Planck system, which is used to determine the evolution of the solvent such that it is not necessary to introduce additional voids [16, 35]. The model has already been verified with fundamental experiments on single-crystal interfaces for the application of metal-electrolyte interfaces [35]. The material modeling is based on the derivation of the free energy density, which allows different system properties within different phases, such as the intracellular or extracellular, to be taken into account.

Our work puts a special emphasis on a consistent modeling of the selectivity filter within the ion channel. The selectivity filter is a crucial structural element that governs the highly selective movement of specific ions across the cell membrane [46,54]. Only certain ions are allowed to pass through the cell membrane, which maintains ion homeostasis and regulates various cellular processes. A key feature of the selectivity filter is its narrow pore region lined with specific amino acids or residues that form a highly structured environment. The size and shape of the pore dictate which ions can pass through, as it must accommodate the size and coordination requirements of the preferred ion. The selectivity filter

is designed to coordinate and stabilize specific ions through electrostatic interactions and coordination bonds. These interactions help to overcome the energetic barrier that ions encounter when moving through the hydrophobic membrane. Each type of ion channel exhibits distinct ion selectivity, favoring the passage of certain ions over others. For instance, Ca^{2+} ion channels will preferentially allow the passage of calcium ions, while K^+ ion channels will primarily facilitate the movement of potassium ions. Notably, the amino acid residues that form the selectivity filter are often highly conserved among members of the same ion channel family, highlighting their crucial functional role and evolutionary significance. In some ion channels, the selectivity filter can also participate in the gating process, regulating the opening and closing of the channel in response to various stimuli, such as changes in membrane voltage or ligand binding. Overall, the selectivity filter in biological ion channels is a finely tuned structure that ensures the precise regulation of ion flux, enabling cells to maintain electrical and chemical gradients essential for cellular function and signaling.

We include the selectivity filter as a separate phase to ensure the consistency of the whole model. The narrowest part of the filter is about the same size as the desolvated ions. Before the solvated ions enter the selectivity filter, they strip off the hydration shell. This phenomenon is accounted for by surface reactions at the interfaces between the outer (inner) region and the selectivity filter region. The electrostatic forces are integrated by a backbone charge and a surface charge.

In section 2 the model framework is presented. The considered domain consists of different phases such as the electrolyte, the lipid bilayer and the selectivity filter (section 2.1). Different species with different properties can be assigned to each phase (section 2.2). The derivation of the chemical potential functions is explained in more detail in section 2.3. In section 2.4 the general system of equations is discussed. We consider different classes of boundary conditions (section 2.5) and due to some equilibrium assumptions the model can be reduced (section 2.6). Furthermore, the scaling of the system is presented to identify important parameters that contribute to the dynamics (section 2.7). In section 3 present our results on the impact and function of the selectivity filter and discuss comparisons to experimental data.

2 General model framework

Our model includes different important aspects of the ion channel and its microenvironment. An illustration of the main features is given in Figure 1. In the extra- and intracellular fluids we find a mixture of different species: anions, cations and solvent molecules. The ions are present in the electrolyte in solvated form. The surface charges of the lipid bilayer and the channel protein lead to the formation of electrical double layers (EDLs). The selectivity filter is located in the channel pore, where charge transfer and desolvation reactions are expected at the interfaces. This leads to different chemical properties and mobilities of the ions in this area. Finally, we can calculate the current I flowing from one bath to the other by

$$I = F \sum_{\alpha=0}^{N} \int_{S^0} z_\alpha \mathbf{J}_\alpha \cdot \mathbf{n} \, \mathrm{dA}, \tag{1}$$

where $S^0 \subset S^j$ is a subset of the Dirichlet boundary, F is the Faraday constant, z_α is the charge number, and $\mathbf{J}_\alpha$ is the flux. This becomes important when studying current-voltage (IV) relations for different membrane potentials E

$$E = \varphi^{\mathrm{in}} - \varphi^{\mathrm{out}}, \tag{2}$$

with φ^{out} and φ^{in} being the potentials at the top and the bottom Dirichlet boundary condition, respectively.

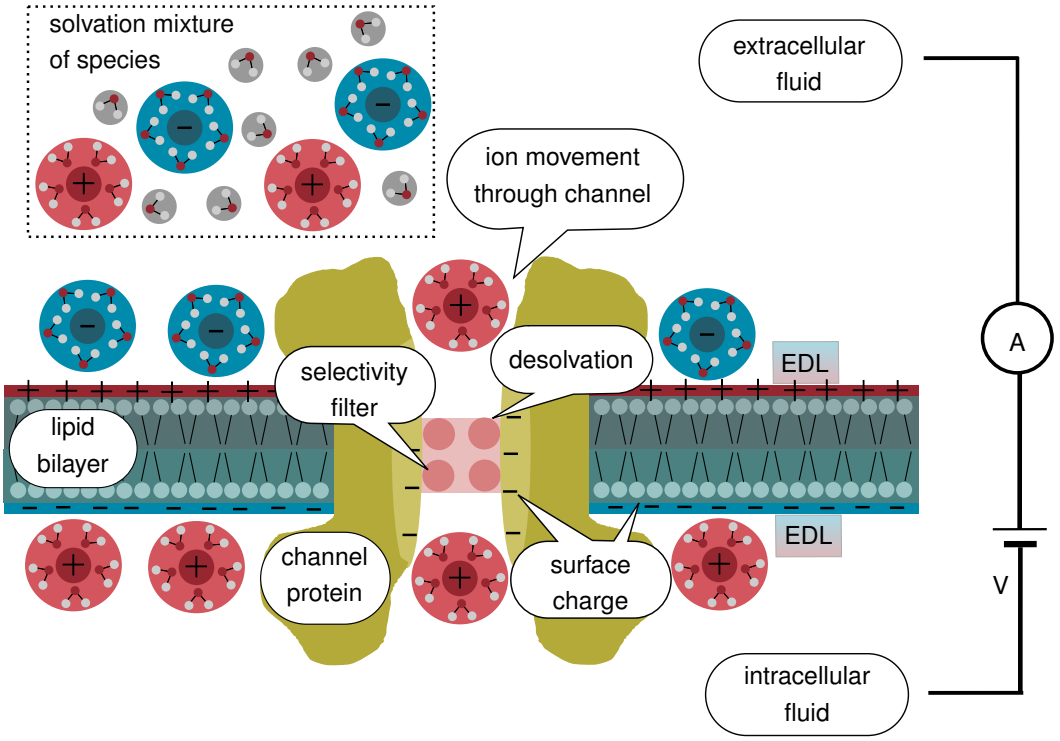

Figure 1: Illustration of an ion channel.

2.1 Domains

We consider a cylindrical, rotationally symmetric domain $\Omega \in \mathbb{R}^3$ that is separated into different phases Ω^j, $j \in \mathcal{J}_\Omega := \{\text{out}, \text{in}, \text{SF}, \text{lip}\}$. At the top we have the outer bath Ω^{out} and at the bottom the inner bath Ω^{in}, both are separated by an impermeable lipid bilayer Ω^{lip}. Inside this membrane there is a single pore, the ion channel, which allows the exchange of particles between the two baths. Within the pore there is an additional domain which controls actual phyisco-chemical processes occuring inside this ion channel, termed selecivity filter Ω^{SF}. An illustration is given in Figure 2.

The domains Ω^j, $j \in \mathcal{J}_\Omega$ share several common interfaces $S^{j,k}$, $j, k \in \mathcal{J}_\Omega, j \neq k$, e.g. the interface $S^{\text{out,SF}}$ between the outer domain and the selectivity filter. The evaluation of some quantity u at the j-side of an interface $S^{j,k}$ will, in general, be written as $u|_j^{j,k}$, for instance, $u|_{\text{out}}^{\text{out,SF}}$. If the interface is an actual boundary of a domain to the exterior, i.e. S^{out}, then $u|^{\text{out}}$ is the evaluation of u at S^{out} approaching always from within the corresponding domain. In order to compactify the typeface, we will also use the typeface $u|_j^{j,k} = u|_+^{j,k}$ and $u|_k^{j,k} = u|_-^{j,k}$. Hence we define the jump brackets $[\![u]\!]^{j,k} := u_+^{j,k} - u_-^{j,k}$, $j, k \in \mathcal{J}_\Omega$. If no index ^{j,k} is given for the interface, then it is assumed to be implicitly clear from the context.

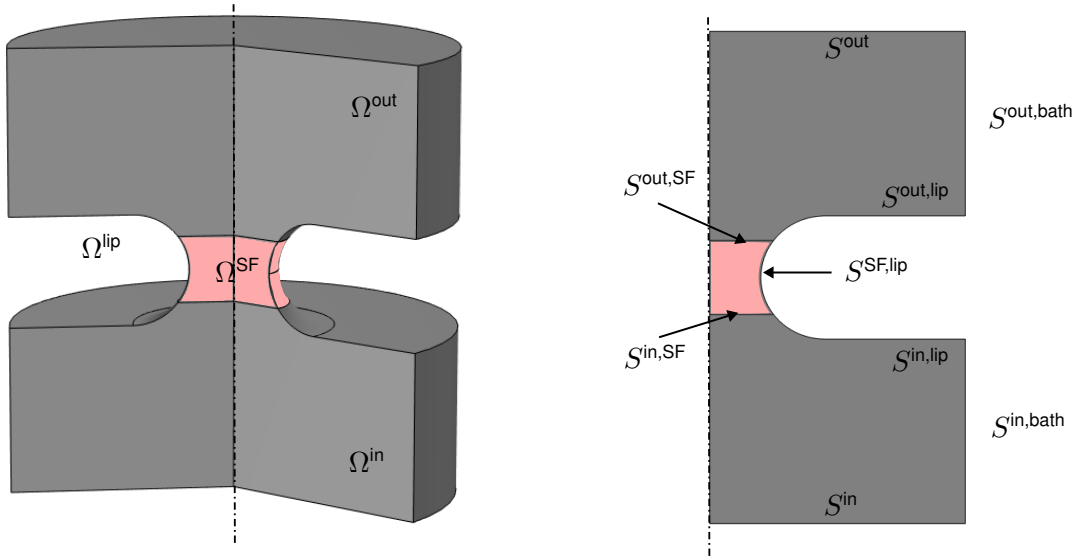

Figure 2: Illustration of the geometric domain. The top and the bottom bath (gray areas) are separated by an impermeable membrane (cut out) that contains a single pore. Inside the pore is the selectivity filter (SF) embedded as an additional domain (pink area). The full domain Ω is split into outer bath Ω^{out}, the inner bath Ω^{in}, the lipid bilayer Ω^{lip}, and the selectivity filter domain Ω^{SF}.

2.2 Species

In each region $(\Omega^j)_{j\in\mathcal{J}_\Omega}$ we consider a mixture of anions, cations, solvent molecules and additional species. Each mixture contains $N^j, j \in \mathcal{J}_\Omega$, different constituents A^j_α with $\alpha \in \mathcal{I}^j \subset \mathbb{N}^+_0$. Quite frequently, the solvent is denoted by A_0, if present. The constituents have molar masses m^j_α, molar volumes v^j_α and carry a charge $z^j_\alpha e_0$, where e_0 is the elementary charge. We emphasize that the ionic species are subject to solvation effects, whereby m^j_α and v^j_α denotes the mass and volume of the solvated ions, respectively [34, 35]. Hence, the molar mass writes as $m^j_\alpha = \tilde{m}_\alpha + \kappa^j_\alpha m^j_0$ since mass is conserved upon solvation, where $\tilde{m}_\alpha$ is the mass of the central ion, κ^j_α the number of solvent molecules bound to the ion, and m^j_0 the mass of the solvent molecule. For the partial molar volume of the solvated ions, a similar relation expectably holds, but the volume is not necessarily conserved upon solvation, whereby we have $v^j_\alpha \approx \tilde{v}_\alpha + \kappa^j_\alpha v^j_0$ with the molar volume $\tilde{v}_\alpha$ of the central ion and v^j_0 of the solvent. A convenient, useful and meaningful approximation is for example $\frac{m^j_\alpha}{m^j_0} = \frac{v^j_\alpha}{v^j_0}$ [35]. The molar density for species $A^j_\alpha, \alpha \in \mathcal{I}^j$ is denoted as $n_\alpha(\mathbf{x}, t)$ for $\mathbf{x} \in \Omega^j with j \in \mathcal{J}_\Omega$. Further, the mass density $\rho^j(\mathbf{x}, t)$ and the charge density $q^j(\mathbf{x}, t)$ are given by

$$\rho^j = \sum_{\alpha\in\mathcal{I}^j} m^j_\alpha n_\alpha \quad \text{and} \quad q^j = F \sum_{\alpha\in\mathcal{I}^j} z^j_\alpha n_\alpha \,.$$

2.3 Chemical potential functions

For each constituent A^j_α, we have a chemical potential μ^j_α, which is determined from the free energy density $\rho\psi^j$ of the mixture in the respective phase $\Omega^j, j \in \mathcal{J}_\Omega$, i.e.,

$$\mu^j_\alpha := \frac{\partial(\rho\psi^j)}{\partial n_\alpha}, \quad \forall\alpha \in \mathcal{I}^j. \tag{3}$$

(a) (b)

Figure 3: Illustration of the solvation effect for (a) a monovalent cation such as sodium Na^+ and (b) a monovalent anion such as Cl^-.

Note, that the above syntax with superscript ^{j} allows to distinguish for a specific ion, e.g. Ca^{2+}, its actual state in the various phases of our system Ω. For example, the constituent Ca^{2+} is solvated in the electrolytic domain Ω^{in} but desolvated in Ω^{SF}. To account for this, we have to denote Ca^{2+} in Ω^{in} as $Ca^{2+,\text{in}}$ and Ca^{2+} in Ω^{SF} as $Ca^{2+,\text{SF}}$, and consequently all the corresponding material functions such as n_α or μ_α. If, for a given species, the assignment is unique, we drop the index ^{j}.

2.3.1 Electrolyte domains

We consider the electrolyte domains Ω^{in} and Ω^{out} as liquid mixtures of several charged and uncharged constituents. The charged ions are subject to the solvation effect, which is of major importance for the electrolytic material models [34, 35]. The free energy density $\rho\psi^j, j = \{\text{in}, \text{out}\}$ can then be written as

$$\rho\psi^j\left(T, n_0, \dots, n_N, \mathbf{E}\right) = \rho\psi^{j,\text{pol}} + \rho\psi^{j,\text{mech}} + \rho\psi^{j,\text{mix}} + \rho\psi^{j,\text{ref}}, \tag{4}$$

where

$$\rho\psi^{j,\text{pol}} = -\frac{1}{2}\varepsilon_0\chi|\mathbf{E}|^2 \tag{5}$$

is the contribution due to polarization of the mixture,

$$\rho\psi^{j,\text{mech}} = \left(K^j - p^R\right)\left(1 - H^j\right) + K^j H^j \ln\left(H^j\right), \tag{6}$$

with $H^j = \sum_{\alpha\in\mathcal{I}^j} v_\alpha^j n_\alpha$ and the bulk modulus K^j, is the mechanical contribution,

$$\rho\psi^{j,\text{mix}} = RT \sum_{\alpha\in\mathcal{I}^j} n_\alpha \ln\left(y_\alpha\right), \tag{7}$$

with $y_\alpha := \frac{n_\alpha}{n}$ is the free energy contribution due to the entropy of mixing, and

$$\rho\psi^{j,\text{ref}} = \sum_{\alpha\in\mathcal{I}^j} g_\alpha^j\, n_\alpha, \tag{8}$$

with $g_\alpha^j = \text{const.}$ is the reference state contribution.

In the in-compressible limit $K^j \to \infty$, this yields the chemical potential function

$$\mu_\alpha^j = g_\alpha^j + RT \ln\left(y_\alpha\right) + v_\alpha^j\, p\,, \tag{9}$$

where v_α^j denotes the partial molar volume of the (solvated) constituent in the phase Ω^j, p the material pressure, R the gas constant and T the temperature. A detailed derivation of the chemical potential is given in [15, 16]. The in-compressible limit $K \to \infty$ entails further the *incompressibility constraint*

$$\sum_{\alpha \in \mathcal{I}^j} v_\alpha^j n_\alpha = 1 \,, \tag{10}$$

which allows us to express

$$n = \sum_{\alpha \in \mathcal{I}^j} n_\alpha = \frac{1}{v_0} + \sum_{\alpha \in \mathcal{I}^j \setminus 0} \left(1 - \frac{v_\alpha}{v_0}\right) n_\alpha = n_0^{\text{ref}} + \sum_{\alpha \in \mathcal{I}^j \setminus 0} \left(1 - n_0^{\text{ref}} v_\alpha\right) n_\alpha \,, \tag{11}$$

and

$$y_\alpha = \frac{n_\alpha}{n_0^{\text{ref}} + \sum_{\beta \in \mathcal{I}^j \setminus 0} (1 - n_0^{\text{ref}} v_\beta) n_\beta} \,, \tag{12}$$

where $n_0^{\text{ref}} = \text{const.}$ is the reference molar density of the pure solvent, e.g. $n_0^{\text{ref}} = 55.5\,\text{mol}\,\text{L}^{-1}$.

2.3.2 Selectivity filter

The selectivity filter is essentially considered as a solid or polymeric electrolyte. We focus here on a rather simplistic material function for the free energy density $\rho\psi^{\text{SF}}$ of the selectivity filter, since the scope of this work is to show its general impact. In subsequent studies we will discuss various material models for $\rho\psi^{\text{SF}}$ and show its impact on the overall behavior of the ion channel.

We consider a free energy density $\rho\psi^{\text{SF}} = \rho\psi^{\text{SF,ref}} + \rho\psi^{\text{SF,mix}} + \rho\psi^{\text{SF,mech}}$ with reference contribution of the pure substances $\rho\psi^{\text{SF,ref}}$, mixing entropy contribution $\rho\psi^{\text{SF,mix}}$ and mechanical contribution $\rho\psi^{\text{SF,mech}}$. Note that enthalpy or other chemical contributions arising in polymeric systems can be included here.

The set of species $\mathcal{I}^{\text{SF}}$ which are present in Ω^{SF} decomposes into the *mobile* species $\mathcal{I}^{\text{pass}}$ which are allowed to pass the filter, and the *immobile* $\mathcal{I}^{\text{scaf}}$ species which actually form the *scaffold* structure of the filter and thus the *lattice sites* on which the mobile species may diffuse [35].

We consider thus a mixture of particles on a lattice which is formed by species $\mathsf{A}_\alpha, \alpha \in \mathcal{I}^{\text{scaf}}$ and on which the particles $\mathsf{A}_\alpha, \alpha \in \mathcal{I}^{\text{pass}}$ may mix. Let $\mathcal{N}_\alpha, \alpha \in \mathcal{I}^{\text{SF}}$ denote particle numbers and $\mathcal{N}_\ell = \sum_{\alpha \in \mathcal{I}^{\text{scaf}}} \omega_\alpha \mathcal{N}_\alpha$ the number of lattice sites, whereby ω_α is the number of lattice sites each particle $\mathsf{A}_\alpha, \alpha \in \mathcal{I}^{\text{scaf}}$ provides. Further, we assume that each constituent $\mathsf{A}_\alpha, \alpha \in \mathcal{I}^{\text{pass}}$ requires ω_α sites on the lattice, whereby the number of vacancies (free lattice sites) is

$$\mathcal{N}_\mathcal{V} = \mathcal{N}_\ell - \sum_{\alpha \in \mathcal{I}^{\text{pass}}} \omega_\alpha \mathcal{N}_\alpha . \tag{13}$$

The number of entropically exchangeable particles $\widetilde{\mathcal{N}}$ is hence

$$\widetilde{\mathcal{N}} = \mathcal{N}_\mathcal{V} + \sum_{\alpha \in \mathcal{I}^{\text{pass}}} \mathcal{N}_\alpha \,. \tag{14}$$

This leads to the number of possible configurations[1]

$$W = \begin{pmatrix} \widetilde{\mathcal{N}} \\ \mathcal{N}_1, \ldots, \mathcal{N}_{N^{\text{pass}}}, \mathcal{N}_\mathcal{V} \end{pmatrix} \tag{15}$$

[1] Note that this is the multi-nominal coefficient.

where we assumed $\mathcal{I}^{\text{pass}} = \{1, 2, \ldots, N^{\text{pass}}\}$ for the sake of this derivation. The entropy of mixing is then

$$S = k_{\text{B}} \begin{pmatrix} \widetilde{\mathcal{N}} \\ \mathcal{N}_1, \ldots, \mathcal{N}_{N^{\text{pass}}}, \mathcal{N}_{\mathcal{V}} \end{pmatrix} , \tag{16}$$

which leads in the Stirling approximation to the configuration entropy

$$S = -k_{\text{B}} \left(\sum_{\alpha \in I^{\text{pass}}} \mathcal{N}_\alpha \ln \left(\frac{\mathcal{N}_\alpha}{\widetilde{\mathcal{N}}} \right) + \mathcal{N}_{\mathcal{V}} \ln \left(\frac{\mathcal{N}_{\mathcal{V}}}{\widetilde{\mathcal{N}}} \right) \right) . \tag{17}$$

Transition to particle molar densities $n_\alpha = \frac{\mathcal{N}_\alpha}{V N_A}$, $\alpha = \mathcal{I}^{\text{SF}} \cup \mathcal{V}$, where V denotes the volume of the *mental* box, leads to a configurational entropy contribution of the free energy as

$$\rho\psi^{\text{SF,mix}} = \sum_{\alpha \in \mathcal{I}^{\text{pass}}} n_\alpha \, RT \ln \left(\frac{n_\alpha}{\tilde{n}} \right) + n_{\mathcal{V}} \, RT \ln \left(\frac{n_{\mathcal{V}}}{\tilde{n}} \right) . \tag{18}$$

with

$$\tilde{n} = \sum_{\alpha \in \mathcal{I}^{\text{pass}}} n_\alpha + n_{\mathcal{V}} , \qquad \text{the number of mixing particles on the lattice,} \tag{19}$$

$$n_\ell = \sum_{\alpha \in \mathcal{I}^{\text{scaf}}} \omega_\alpha n_\alpha , \qquad \text{the number of lattice sites,} \tag{20}$$

$$n_{\mathcal{V}} = n_\ell - \sum_{\alpha \in \mathcal{I}^{\text{pass}}} \omega_\alpha n_\alpha , \qquad \text{the number of vacancies,} \tag{21}$$

$$y_\alpha := \frac{n_\alpha}{\tilde{n}}, \; \alpha \in \{\mathcal{I}^{\text{pass}}, \mathcal{V}\}, \qquad \text{the lattice fraction ,} \tag{22}$$

where $\omega_\alpha, \alpha \in \mathcal{I}^{\text{scaf}}$ is the number of lattice sites each constituent A_α delivers and $\omega_\alpha, \alpha \in \mathcal{I}^{\text{pass}}$ is the number of lattice sites each constituent A_α requires on the lattice. Note that for a single diffusive species $y = \frac{n_\alpha}{\tilde{n}}$ requiring one lattice site, one obtains the simple lattice entropy of mixing

$$\rho\psi^{\text{SF,mix}} = n_\ell RT \left(y \ln (y) + (1-y) \ln (1-y) \right) . \tag{23}$$

The mechanical contribution is considered as

$$\rho\psi^{\text{SF,mech}} = \left(K^{\text{SF}} - p^R \right) \left(1 - H^{\text{SF}} \right) + K^{\text{SF}} H^{\text{SF}} \ln \left(H^{\text{SF}} \right) , \tag{24}$$

with $H^{\text{SF}} = \sum_{\alpha \in \mathcal{I}^{\text{scaf}}} v_\alpha^{\text{SF}} n_\alpha$, whereby only the *immobile* species contribute to the mechanical energy. The reference contribution is similar to the electrolyte considered as

$$\rho\psi^{\text{ref}} = \sum_{\alpha \in \mathcal{I}^{\text{SF}}} g_\alpha^{\text{SF}} \, n_\alpha . \tag{25}$$

In the incompressible limit $K^{\text{SF}} \to \infty$, we obtain the chemical potential functions

$$\mu_\alpha^{\text{SF}} = \frac{\partial \rho\psi^{\text{SF}}}{\partial n_\alpha} = \begin{cases} g_\alpha^{\text{SF}} + RT \, \omega_\alpha \ln (y_{\mathcal{V}}) + v_\alpha^{\text{SF}} \, p + RT \, \omega_\alpha \left(1 - y_\nu - \sum_{\beta \in \mathcal{I}^{\text{pass}}} y_\beta \right) , & \alpha \in \mathcal{I}^{\text{scaf}} \\ g_\alpha^{\text{SF}} + RT \ln (y_\alpha) - RT \, \omega_\alpha \ln (y_{\mathcal{V}}) + RT \, (1 - \omega_\alpha) \, (1 - y_\alpha - y_\nu) , & \alpha \in \mathcal{I}^{\text{pass}} \end{cases} \tag{26}$$

where p denotes again the material pressure.

For the sake of simplicity we consider in the following that the lattice is built by a single species $\mathsf{A}_0^{\mathsf{SF}}$ whereby $n_\ell = \omega_0 n_0^{\mathsf{SF}}$. Further, we assume that all species which are allowed to pass require only a single site, which employs $\omega_\alpha = 1, \alpha \in \mathcal{I}^{\mathsf{pass}}$. The lattice fraction of the vacancies can be rewritten as $y_\mathcal{V} = 1 - \sum_{\beta\in\mathcal{I}^{\mathsf{pass}}} y_\beta$, where $\tilde{n} = n_\ell =$const.. Further, we assume that $\mathsf{A}_0^{\mathsf{SF}}$ is in equilibrium whereby $\nabla\mu_0 = 0$. Hence, we have for the diffusional flux $\hat{\mu}_\alpha^{\mathsf{SF}} = \mu_\alpha^{\mathsf{SF}}$ with

$$\mu_\alpha^{\mathsf{SF}} = g_\alpha^{\mathsf{SF}} + RT\ln(y_\alpha) - RT\ln\left(1 - \sum_{\beta\in\mathcal{I}^{\mathsf{pass}}} y_\beta\right), \alpha \in \mathcal{I}^{\mathsf{pass}} \tag{27}$$

Since $\hat{\mu}_\alpha = \mu_\alpha((y_\beta)_{\beta\in\mathcal{I}^{\mathsf{pass}}})$, the Poisson equation and the momentum equation decouple, and only the Poisson equation and the transport balance are needed. However, the momentum balance is yet valid and serves to determine the pressure *a posteriori*.

Regarding the *backbone charge* of the *scaffold* structure, some cases have to be considered:

- backbone is uncharged, whereby

$$q^{\mathsf{SF}} = F\sum_{\alpha\in\mathcal{I}^{\mathsf{pass}}} z_\alpha^{\mathsf{SF}} n_\alpha \tag{28}$$

- backbone is fully charged, whereby

$$q^{\mathsf{SF}} = F\sum_{\alpha\in\mathcal{I}^{\mathsf{pass}}} z_\alpha^{\mathsf{SF}} n_\alpha + F z_{n_\ell} n_\ell \tag{29}$$

  and $z_{n_\ell} < 0$. Note that q^{SF} has then a constant backbone volume charge, similar like a solid electrolyte. This has to satisfy then (integrate poisson equation, initial state is that there are no A_α, $\alpha \in \mathcal{I}^{\mathsf{pass}}$ present within Ω^{SF})

$$F z_{n_\ell} n_\ell \,\mathsf{vol}(\Omega^{\mathsf{SF}}) \overset{!}{=} \underset{s}{q}^{\mathsf{SF,lip}}\,\mathsf{area}(S^{\mathsf{SF,lip}}) , \tag{30}$$

  where $\underset{s}{q}^{\mathsf{SF,lip}}$ is the surface charge of the channel protein within the selectivity filter.

- an intermediate state, whereby

$$F z_0^{\mathsf{SF}} n_\ell \,\mathsf{vol}(\Omega^{\mathsf{SF}}) \overset{!}{=} \zeta\, \underset{s}{q}^{\mathsf{SF,lip}}\mathsf{area}(S^{\mathsf{SF,lip}}) , \tag{31}$$

  with some scaling parameter ζ.

Note that electroneutrality must also be ensured in the selectivity filter when charged species are present and backbone and surface charges are considered.

2.3.3 Lipid bilayer

The lipid bilayer is a thin polar membrane composed of amphiphilic lipids. Especially in the gating process of mechano-sensitive ion channels, the deformation of the lipid bilayer plays a crucial role. For example, the opening probability responds to mechanical stimulation of the channel protein such as cell-stretch [33].

However, within this work, the membrane is not explicitly modeled but is included through boundary conditions. Its impermeability to ions is described by a no-flux boundary condition, and its surface charge can be accounted for by a Neumann boundary condition (see section 2.5). The inclusion of an elastic lipid bilayer is the subject of future work.

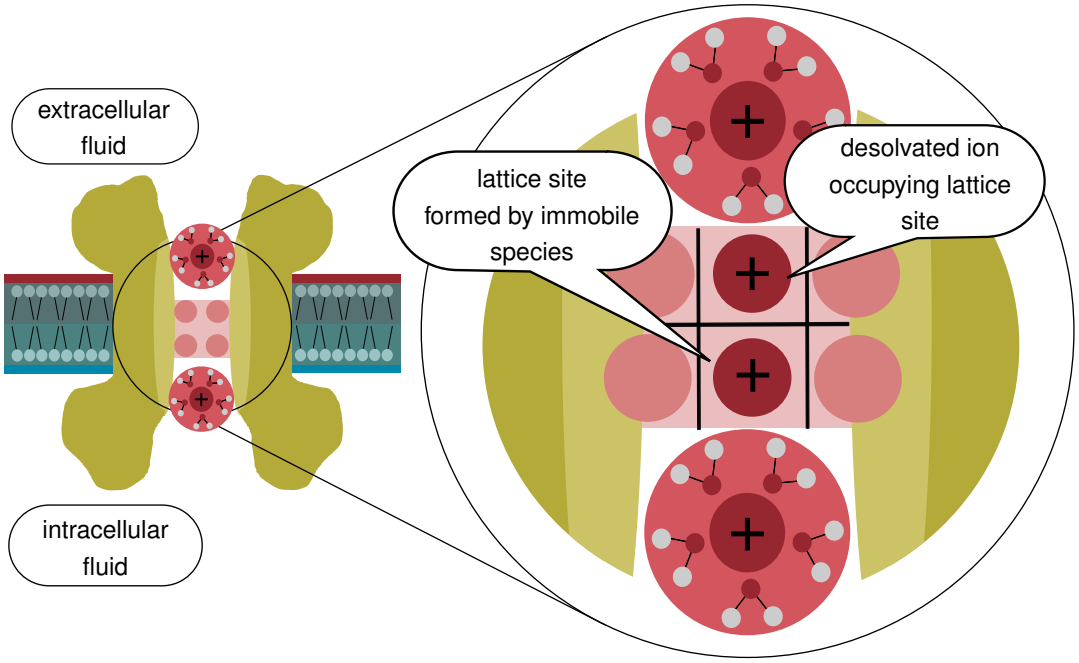

Figure 4: Illustration of the selectivity filter domain. The immobile species form lattice sites on which the mobile species may diffuse.

2.4 Balance equations

In the following, we assume that the process is isothermal, i.e., the temperature T is constant. The evolution of the molar densities $n_\alpha(\mathbf{x},t)$ for $\alpha \in (\mathcal{I}^j)_{j\in\mathcal{J}_\Omega}$, the electrostatic potential $\varphi(\mathbf{x},t)$ and the barycentric velocity $\mathbf{v}(\mathbf{x},t)$ for $\mathbf{x} \in (\Omega^j)_{j\in\mathcal{J}_\Omega}$, are described by

$$\partial_t n_\alpha + \nabla\cdot(n_\alpha \mathbf{v} + \mathbf{J}_\alpha) = 0 \tag{32}$$

$$-\nabla\cdot\left[\varepsilon_0\left(1+\chi^j\right)\nabla\varphi\right] = q^j, \tag{33}$$

$$\partial_t \rho^j + \nabla\cdot\left(\rho^j\mathbf{v}\right) = 0, \tag{34}$$

$$\partial_t\left(\rho^j\mathbf{v}\right) + \nabla\cdot(\rho\mathbf{v}\otimes\mathbf{v} - \Sigma) = 0. \tag{35}$$

Note that diffusional fluxes $\mathbf{J}_\alpha$ in (32) are subject to the constraint

$$\sum_{\alpha\in\mathcal{I}^j} m_\alpha^j \mathbf{J}_\alpha = 0\,. \tag{36}$$

If the species A_0 is mobile, this condition can be exploited to show, based on nonequilibrium thermodynamics [12], that the flow is driven by the diffusive chemical potential $\hat{\mu}_\alpha^j = \mu_\alpha^j - \frac{m_\alpha^j}{m_0^j}\mu_0^j$, as well as by the electrostatic potential φ, and is given by

$$\mathbf{J}_\alpha = -\sum_{\beta\in\mathcal{I}^j} M_{\alpha\beta}^j\left(\nabla\hat{\mu}_\beta^j + e_0 z_\beta^j\nabla\varphi\right), \quad \forall\alpha\in\mathcal{I}^j, j\in\mathcal{J}_\Omega, \tag{37}$$

where the mobility matrix $M_{\alpha,\beta}^j$ must be positive definite. The total mass flux of a species A_α is denoted by $\mathbf{j}_\alpha := n_\alpha\mathbf{v} + \mathbf{J}_\alpha$. In the Poisson equation (33), we denote with ε_0 the vacuum permittivity and with χ^j the dielectric susceptibility, which is assumed to be constant throughout this work. Note, however, that χ^j can itself be dependent on the (local) species densities as well as on the electric

field [36]. The total stress Σ in the momentum balance equation (35) consits of the material stress tensor σ^{visc} and the Maxwell stress tensor, arising from the electromagnetic field, and is defined as

$$\Sigma = \sigma^{\text{visc}} - \left(p + \frac{1}{2}\epsilon_0(1+\chi)|\mathbf{E}|^2 \right) \mathbf{1} + \epsilon_0(1+\chi)\mathbf{E} \otimes \mathbf{E}, \tag{38}$$

with the material pressure p, the electric field $\mathbf{E} = -\nabla\varphi$, and the identity matrix $\mathbf{1}$. Note again that additional terms arise in the Maxwell stress tensor when χ^j is concentration- or field-dependent [36].

Besides the Poisson equation (33), in some situations it is convenient to consider also the charge balance equation

$$\partial_t q^j + \nabla \cdot (q^j \mathbf{v} + \mathbf{J}_q) = 0 \tag{39}$$

where $\mathbf{J}_q = e_0 \sum_{\alpha \in \mathcal{I}^j} z_\alpha^j \mathbf{J}_\alpha$ is the (diffusional) electric charge and $\mathbf{j}_q := q^j \mathbf{v} + \mathbf{J}_q$ the total charge of the system.

2.5 Boundary conditions

We have to specify boundary conditions essentially at the interfaces S^{out}, S^{in}, $S^{\text{out,SF}}$, $S^{\text{in,SF}}$, $S^{\text{SF,lip}}$, $S^{\text{out,lip}}$ and $S^{\text{in,lip}}$. For the rest of $\partial\Omega$ we will assume homogeneous Neumann boundary conditions, which arise essentially from the rotational symmetry of the problem.

Several classes of boundary conditions at an interface S^j can be defined. For the constituents A_α^j, three types of boundary conditions arise:

1 prescribed concentrations in the bulk, i.e. $n_\alpha|^j = n_\alpha^j = \text{const.}$[2] *Concentration-Dirichlet boundary conditions (CD-BCs)*,

2 prescribed fluxes, i.e. $\mathbf{j}_\alpha \cdot \mathbf{n}|^j = j_\alpha^j = \text{const.}$, termed *Concentration Flux boundary conditions (CF-BCs)*, with the special case $\mathbf{j}_\alpha \cdot \mathbf{n}|^j = 0$ called *No-Flux boundary condition (NF-BCs)* or *homogeneous Neumann boundary condition*,

3 *surface reaction boundary conditions (SR-BCs)* $\mathbf{j}_\alpha \cdot \mathbf{n}|^{j,k} = \underset{s}{R}((n_\beta^j)_{\beta\in\mathcal{I}^j}, (n_\beta^k)_{\beta\in\mathcal{I}^k})$.

For the electrostatic potential φ or the charge q^j, we have the following three types of boundary conditions:

1 prescribed electrostatic potential in the bulk, i.e. $\varphi|^j = \varphi^j = \text{const.}$[3], termed *Potential Dirichlet boundary conditions (PD-BCs)*,

2 continuity of the electrostatic potential, i.e. $[\![\varphi]\!]^j = 0$, termed *potential continuity boundary condition (PC-BC)*,

3 prescribed surface charge density, i.e. $[\![\varepsilon_0(1+\chi)\nabla\varphi]\!]\mathbf{n}|^j = \underset{s}{q^j}$, called *surface charge boundary condition (SC-BCs)* with the special case $\underset{s}{q^j} = 0$ termed *no charge boundary condition (NC-BCs)*,

4 a prescribed electrical current, i.e. $\mathbf{j}_q \cdot \mathbf{n}|^j = i_q^j$[4], which we call electric current boundary

[2] Note that constant refers here to *constant* with respect to all other state-variables. However, n_α^j could be, for instance, time-dependent

[3] Note that constant refers here to *constant* with respect to all other state-variables. However, φ could be, for instance, time-dependent

[4] similar to above, i_q could be time-dependent

condition (EC-BCs).

Briefly note that, even if we prescribe for some quantity u at a certain boundary S^j its value, i.e. $u|^j = u^j$, we can still evaluate (*a posteriori*, e.g. by numerical simulations) its flux through the boundary, e.g. $\mathbf{j}_u \cdot \mathbf{n}|^j$. In order to distinguish this from prescribed values, we denote such an *a posteriori* by $\mathbf{j}_u \cdot \mathbf{n}|^j = \check{j}_u^j$.

On the top bath S^{out} we consider throughout the whole work (CD-BCs) for all species and (PD-BCs), i.e.

$$n_\alpha|^{\text{out}} = n_\alpha^{\text{out}} \qquad \forall\, \alpha \in \mathcal{I}^{\text{out}}\,, \quad \varphi|^{\text{out}} = \varphi^{\text{out}}\,. \tag{40}$$

This models the outer region as an (*infinite*) bulk solution in which an idealized, non-interacting electrode is placed.

At the bottom boundary S^{in} we we consider essentially two cases,

1 (CD-BC) and (PD-BC), i.e.

$$n_\alpha|^{\text{in}} = n_\alpha^{\text{in}} \qquad \forall\, \alpha \in \mathcal{I}^{\text{in}}\,, \quad \varphi|^{\text{in}} = \varphi^{\text{in}}\,, \tag{41}$$

and thus also an (*infinite*) bulk solution with an idealized, non-interacting electrode is placed.

2 (NF-BC) and (NC-BC), which models Ω^{in} as a closed interior domain, e.g. of a cell, whereby we have

$$\mathbf{j}_\alpha \cdot \mathbf{n}|^{\text{in}} = 0 \quad \forall \alpha \in \mathcal{I}^{\text{in}}, \quad \nabla\varphi \cdot \mathbf{n}|^{\text{in}} = 0. \tag{42}$$

On the boundary $S^{\text{in,bath}}$ and $S^{\text{out,bath}}$ (NF-BCs) and (NC-BCs). On the walls $S^{\text{in,lip}}$ and $S^{\text{out,lip}}$ of the lipid bilayer adjacent to the respective electrolyte domains Ω^{in} and Ω^{out} we consider throughout this work (NF-BC) and (NC-BC), which accounts for electrostatic interactions between the surface charges of the lipid and the ions of the electrolytic solutions, but prohibits chemical reactions of the electrolytic species with the lipid. We have hence ($j = \{\text{in}, \text{out}\}$)

$$\mathbf{j}_\alpha \cdot \mathbf{n}|^{j,\text{lip}} = 0 \quad \forall \alpha \in \mathcal{I}^j, \quad [\![\varepsilon_0(1+\chi)\nabla\varphi]\!] \cdot \mathbf{n}|^{j,\text{lip}} = \underset{s}{q}^{j,\text{lip}} = 0\,, \tag{43}$$

where $\underset{s}{q}^{j,\text{lip}}$ is the charge of the lipid bilayer. On the channel wall $S^{\text{SF,lip}}$, we consider throughout this work (NF-BC) for all constituents and (SC-BC), which again accounts only for electrostatic interactions. To investigate pH effects on the ion channel, it might be necessary to switch to (SC-BC) for species like H^+ or OH^-, but this is subject to a subsequent work. Hence we consider the following boundary conditions,

$$\mathbf{j}_\alpha \cdot \mathbf{n}|^{\text{SF,lip}} = 0 \quad \forall \alpha \in \mathcal{I}^{\text{SF}}, \quad [\![\varepsilon_0(1+\chi)\nabla\varphi]\!] \cdot \mathbf{n}|^{\text{SF,lip}} = \underset{s}{q}^{\text{SF,lip}}, \quad \mathbf{v} = 0 \text{ (no slip)}, \tag{44}$$

where $\underset{s}{q}^{\text{lip,SF}}$ is the charge of the channel wall inside the selectivity filter Ω^{SF}.

The interfaces $S^{\text{out,SF}}$ and $S^{\text{in,SF}}$ between the electrolytic domain and the selectivity filter accounts for the desolvation and resolvation of the ionic species, which is modeled via (SR-BCs), as well as for the selection which ions are not allowed to pass, which is modeled by (NF-BCs). Further, the electrostatic potential is assumed to be continuous across these interfaces, whereby we employ (PC-BCs) for φ.

For a selection of species $\alpha \in \mathcal{I}^{\text{pass}} \subset \{\mathcal{I}^{\text{out}} \cap \mathcal{I}^{\text{in}}\}$ we consider the (de-)solvation and transfer reaction ($j = \{\text{out}, \text{in}\}$)

$$\mathsf{A}_\alpha^j \rightleftharpoons \mathsf{A}_\alpha^{\text{SF}} + \kappa_\alpha \mathsf{A}_0^j, \tag{45}$$

with reaction rate $\underset{s}{r}_\alpha^{\text{pass},j}$. The corresponding surface affinity $\underset{s}{\lambda}^{\text{pass},j}$ for the reaction is

$$\underset{s}{\lambda}_\alpha^{\text{pass},j} := \mu_{\mathsf{A}_\alpha}\big|^{\text{SF}} + \kappa_\alpha \mu_{\mathsf{A}_0}\big|^j - \mu_{\mathsf{A}_\alpha}\big|^j, \tag{46}$$

whereby we can write the reaction rate as [17, 35, 37]

$$\underset{s}{r}_\alpha^{\text{pass},j} = \underset{s}{L}_\alpha^{\text{pass},j}\, g_\alpha\left(\frac{\underset{s}{\lambda}_\alpha^{\text{pass},j}}{RT}\right) \quad \text{with} \quad g_\alpha(z) := \mathrm{e}^{\beta_\alpha z} - \mathrm{e}^{-(1-\beta_\alpha) z}\ . \tag{47}$$

We assume throughout this work, that the solvent species A_0 is not allowed to pass through the selectivity filter, whereby $0 \notin \mathcal{I}^{\text{pass}}$. This is not a necessary restriction of the overall model but a simplification for the sake of this work and may be dropped in subsequent studies. Hence, we can write the reaction boundary conditions as

$$\mathbf{j}_\alpha \cdot \mathbf{n}|_j^{j,\text{SF}} = -\mathbf{j}_\alpha \cdot \mathbf{n}|_{\text{SF}}^{j,\text{SF}} = \underset{s}{r}_\alpha^{\text{pass},j} \qquad \forall \alpha \in \mathcal{I}^{\text{pass}}, \tag{48}$$

$$\mathbf{j}_\alpha \cdot \mathbf{n}|_j^{j,\text{SF}} = 0 \qquad \forall \alpha \in \{\mathcal{I}^{\text{out}} \cup \mathcal{I}^{\text{in}}\} \backslash \{\mathcal{I}^{\text{pass}} \cup 0\}, \tag{49}$$

$$\mathbf{j}_0 \cdot \mathbf{n}|_j^{j,\text{SF}} = \sum_{\alpha \in \mathcal{I}^{\text{pass}}} \kappa_\alpha\, \underset{s}{r}_\alpha^{\text{pass},j}\ . \tag{50}$$

An illustration of the domain including the different boundaries is given in Figure 2. Figure 5 gives

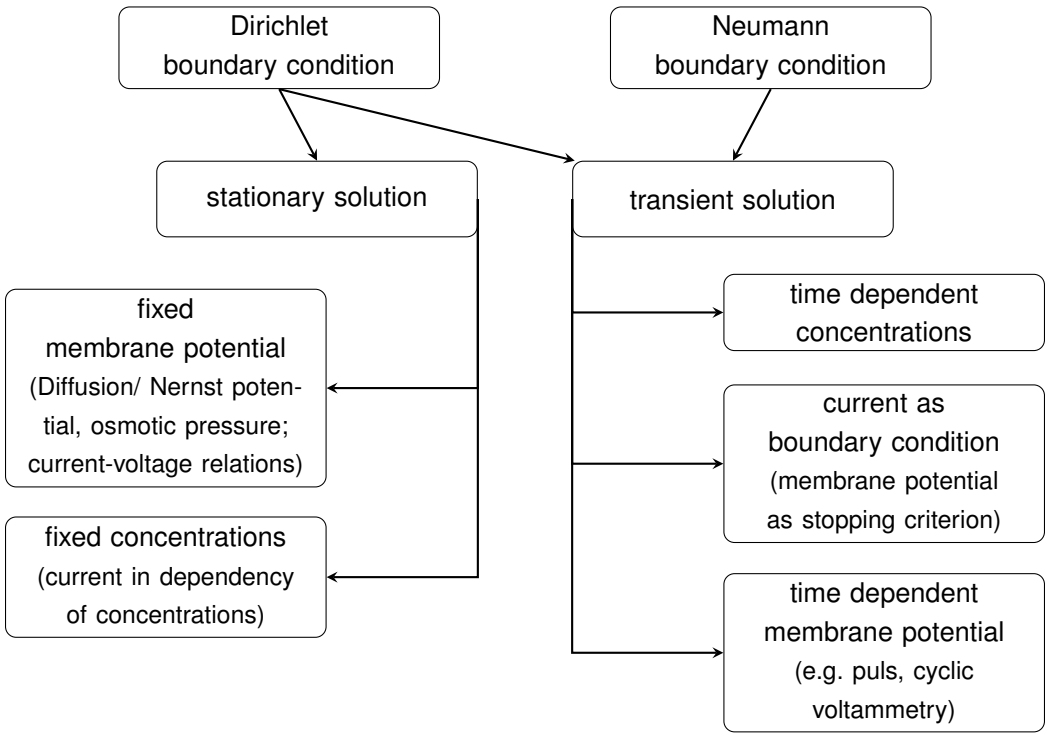

Figure 5: Overview of different boundary conditions that can be applied in the inner region and possible experiments that can be performed.

an overview of the different boundary conditions that can be applied on the exterior of the inner region on S^{in} and their meaning in the context of different experiments. First of all, a distinction can be made between Dirichlet and Neumann boundary conditions. Where (CD-BCs) and (PD-BCs) are usually used to represent single-channel experiments in which two electrolyte buffers are separated by a membrane. This allows the concentrations and the potential to be influenced in the inner and outer domains. Stationary solutions can be obtained, e.g. to calculate currents as a function of concentrations or the membrane potential. It is also possible to calculate time-dependent solutions and, for example, to vary the membrane potential over time, as it is done in voltage-clamp experiments. If in the inner domain (NF-BCs) and (NC-BCs) are applied, one can imagine a scenario in which the ions flow from the outer bath into a closed container (or a cell). Only the concentrations in the outer domain can be varied. To generate a membrane potential, the container or cell must be punctured with a microscopically fine electrode.

2.6 Equilibrium assumptions

In the following some assumptions are elaborated that can be applied in order to reduce the system.

Mechanical equilibrium

We assume that the system is in mechanical equilibrium, such that $\mathbf{v} = 0$ in whole Ω. This reduces the equations (34) and (35) to

$$\nabla p = -q^j \nabla \varphi. \tag{51}$$

Tanking the divergence of both sides yields [22]

$$\nabla \cdot \left[\nabla p + q^j \nabla \varphi\right] = 0. \tag{52}$$

Mobility matrix

The mobility matrices $M_{\alpha\beta}$ are and can in general be functions of the thermodynamic state variables $(n_0, \ldots, n_N)$. For the sake of this work, we consider a Nernst–Einstein-type relation for the diagonal elements,

$$M^j_{\alpha\alpha} = \frac{D^j_\alpha}{RT} n_\alpha. \tag{53}$$

The off-diagonal entries of the mobility matrix $M_{\alpha\beta}$ are chosen to be zero for this work, i.e., $M^j_{\alpha\beta} = 0$ for $\alpha \neq \beta$.

Note that other relations, such as $M^j_{\alpha\alpha} = \frac{D^j_\alpha}{RT} n_\alpha\, y_0$ for the diagonal entries, non-zero off-diagonal entries, which leads to cross-diffusion effects, or general Maxwell-Stefan diffusion relations [7] are also imaginable, thermodynamically consistent and strict forward with the presented model framework.

2.7 Scaling of the equations

In order to express the model in dimensionless quantities we introduce the following substitutions

$$\begin{aligned}
&\mathbf{x} \to L\tilde{\mathbf{x}}, \quad t \to \tau\tilde{t}, n_\alpha \to n^R\tilde{n}_\alpha, \\
&\varphi \to \varphi^R\tilde{\varphi}, \quad p \to p^R\tilde{p}, \quad \hat{\mu}_\alpha^j \to \mu^R\tilde{\mu}_\alpha^j, \\
&\underset{s}{q}^{j,\mathsf{lip}} \to \underset{s}{q}^R\tilde{\underset{s}{q}}^{j,\mathsf{lip}}, \quad \underset{s}{L}_\alpha^{\mathsf{pass},j} \to \underset{s}{L}_\alpha^R\tilde{\underset{s}{L}}_\alpha^{\mathsf{pass},j}.
\end{aligned}$$

The space variable is scaled with the approximate channel width $L = 1\,\mathsf{nm}$, the time variable is scaled with $\tau = 1$ ns and the number densities are scaled with the molar concentration of water $[\mathsf{H_2O}] = 55.5\,\mathsf{mol\,L^{-1}}$. An overview is given in Table 1. All other scalings are chosen such that they drop in the equations. The introduction of the dimensionless quantities in the equations generates

variable	unit	transformation	scaling
$\mathbf{x}$	m	$\mathbf{x} \to L\tilde{\mathbf{x}}$	$L = 1\,\mathsf{nm}$
t	s	$t \to \tau\tilde{t}$	$\tau = 1$ ns
n_α	$\mathsf{mol\,L^{-1}}$	$n_\alpha \to n^R\tilde{n}_\alpha$	$n^R = 55.5\,\mathsf{mol\,L^{-1}}$
φ	V	$\varphi \to \varphi^R\tilde{\varphi}$	$\varphi^R = \frac{RT}{F}$ V
p	Pa	$p \to p^R\tilde{p}$	$p^R = n^RRT$ Pa
$\underset{s}{q}^{j,\mathsf{lip}}$	$\mathsf{C\,m^{-2}}$	$\underset{s}{q}^{j,\mathsf{lip}} \to \underset{s}{q}^R\tilde{\underset{s}{q}}^{j,\mathsf{lip}}$	$\underset{s}{q}^R = Ln^RF\,\mathsf{C\,m^{-2}}$
$L_\alpha^{\mathsf{pass},j}$	$\mathsf{m^{-2}\,s^{-1}}$	$\underset{s}{L}_\alpha^{\mathsf{pass},j} \to \underset{s}{L}_\alpha^R\tilde{\underset{s}{L}}_\alpha^{\mathsf{pass},j}$	$\underset{s}{L}_\alpha^R = \frac{D_\alpha n^R}{L}\,\mathsf{m^2\,s^{-1}}$
$\hat{\mu}_\alpha^j$	J	$\hat{\mu}_\alpha^j \to \mu^R\tilde{\mu}_\alpha^j$	$\mu^R = RT$ J

Table 1: Variable substitutions for nondimensionalization.

three new constants

$$\tilde{D}_\alpha := \frac{D_\alpha\tau}{L^2}, \tag{54a}$$

$$\lambda^2 := \frac{\varphi^R\varepsilon_0(1+\chi)}{L^2n^RF}, \tag{54b}$$

and

$$a_\alpha^2 := \frac{p^R(v_\alpha^j - \frac{m_\alpha^j}{m_0^j}v_0^j)}{RT}. \tag{54c}$$

Dimensionless system

Applying the before introduced properties and assumptions, as well as the scaling of the variables leads to the following system of equations (omitting the tilde for ease of notation)

$$\partial_t n_\alpha + \nabla\cdot\mathbf{J}_\alpha = 0 \quad \forall\alpha \in (\mathcal{I}^j)_{j\in\mathcal{J}_\Omega}, \tag{55a}$$

$$-\lambda^2 \Delta \varphi = q^j, \tag{55b}$$

$$\nabla \cdot \left[\nabla p + q^j \nabla \varphi \right] = 0. \tag{55c}$$

The flux in equation (55a) varies within the different phases. For the outer and inner bath we have with the chemical potential (9) ($j = \{\mathsf{out}, \mathsf{in}\}$)

$$\mathbf{J}_\alpha = -D_\alpha^j n_\alpha \left[\nabla \left\{ \ln\left(\frac{n_\alpha}{n}\right) - \frac{m_\alpha^j}{m_0^j} \ln\left(\frac{n_0}{n}\right) \right\} + a_\alpha^2 \nabla p + z_\alpha^j \nabla \varphi \right] \quad \forall \alpha \in \mathcal{I}^j. \tag{56}$$

For the selectivity filter domain we find with the chemical potential (27)

$$\mathbf{J}_\alpha = -D_\alpha^{\mathsf{SF}} n_\alpha \left[\nabla \left\{ \ln\left(\frac{n_\alpha}{n_\ell}\right) - \ln\left(1 - \sum_{\beta \in \mathcal{I}^{\mathsf{pass}}} \frac{n_\beta}{n_\ell}\right) \right\} + z_\alpha^{\mathsf{SF}} \nabla \varphi \right] \quad \forall \alpha \in \mathcal{I}^{\mathsf{SF}}. \tag{57}$$

Scaled boundary conditions

For the scaled (CD-BCs) and (PD-BCs) on the top S^{out} and the bottom S^{in} boundary we find ($j = \{\mathsf{out}, \mathsf{in}\}$)

$$n_\alpha|^j = \frac{n_\alpha^j}{n^R} \qquad \forall\, \alpha \in \mathcal{I}^j, \quad \varphi|^j = \frac{\varphi^j}{\varphi^R}\,. \tag{58}$$

The surface charge boundary conditions (SC-BC) on $S^{j,\mathsf{lip}}$, $j = \{\mathsf{in}, \mathsf{out}\}$ become

$$[\![\varepsilon_0 (1+\chi) \nabla \varphi]\!] \cdot \mathbf{n}|^{j,\mathsf{lip}} = \frac{\underset{s}{q^{\mathsf{lip}}}}{\underset{s}{q^R} \lambda^2}\,, \tag{59}$$

and on $S^{\mathsf{SF,lip}}$ we get

$$[\![\varepsilon_0 (1+\chi) \nabla \varphi]\!] \cdot \mathbf{n}|^{\mathsf{SF,lip}} = \frac{\underset{s}{q^{\mathsf{SF,lip}}}}{\underset{s}{q^R} \lambda^2}\,. \tag{60}$$

The dimensionless reaction boundary conditions on the interfaces $S^{\mathsf{out,SF}}$ and $S^{\mathsf{in,SF}}$ are given by ($j = \{\mathsf{out}, \mathsf{in}\}$)

$$\mathbf{j}_\alpha \cdot \mathbf{n}|_j^{j,\mathsf{SF}} = -\mathbf{j}_\alpha \cdot \mathbf{n}|_{\mathsf{SF}}^{j,\mathsf{SF}} = \underset{s}{r_\alpha^{\mathsf{pass},j}} \qquad \forall \alpha \in \mathcal{I}^{\mathsf{pass}} \tag{61}$$

$$\mathbf{j}_\alpha \cdot \mathbf{n}|_j^{j,\mathsf{SF}} = 0 \qquad \forall \alpha \in \{\mathcal{I}^{\mathsf{out}} \cup \mathcal{I}^{\mathsf{in}}\} \backslash \{\mathcal{I}^{\mathsf{pass}} \cup 0\} \tag{62}$$

$$\mathbf{j}_0 \cdot \mathbf{n}|_j^{j,\mathsf{SF}} = \sum_{\alpha \in \mathcal{I}^{\mathsf{pass}}} \kappa_\alpha \, \underset{s}{r_\alpha^{\mathsf{pass},j}}\,, \tag{63}$$

with

$$\underset{s}{r_\alpha^{\mathsf{pass},j}} = \underset{s}{L_\alpha^{\mathsf{pass},j}} \, g_\alpha \left(\frac{\underset{s}{\lambda^{\mathsf{pass},j}}}{RT} \right) \quad \text{with} \quad g_\alpha(z) := \mathsf{e}^{\beta_\alpha z} - \mathsf{e}^{-(1-\beta_\alpha) z}\,. \tag{64}$$

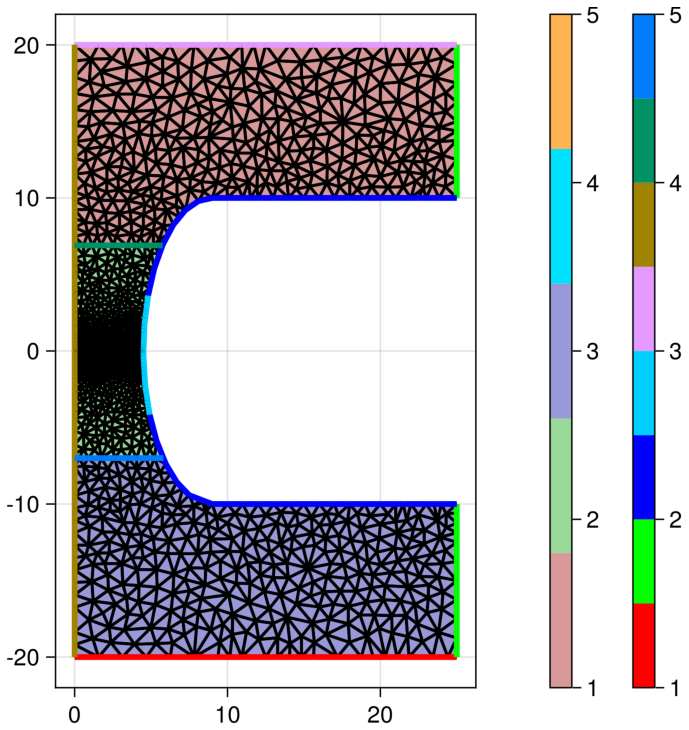

Figure 6: Illustration of the simulation domain. The different phases (left colorbar) and boundaries are marked by different colors (right colorbar). The mesh within the selectivity filter is refined in this area where the surface charge is applied.

2.8 Numerical method

In order to solve the system we use Julia and the VORONOIFVM.JL package [23] which implements the Voronoi cell based finite volume method. The boundary conforming Delaunay triangulation of the domain Ω is generated with the help of the Triangle mesh generator [50]. The transport equation (55a) is discretized using a backward Euler scheme in time. For the flux we use a Scharfetter–Gummel inspired discretization [24, 40]. To do so the excess chemical potential

$$\nu_\alpha(n_0, \dots, n_N, p) := \hat{\mu}_\alpha(n_0, \dots, n_N, p) - \ln(n_\alpha) \tag{65}$$

is introduced to rewrite the flux term as

$$\mathbf{J}_\alpha = -D_\alpha \left[\nabla n_\alpha + n_\alpha \nabla (\nu_\alpha + z_\alpha \varphi)\right]. \tag{66}$$

The term $\nu_\alpha + z_\alpha\varphi$ then replaces the electrostatic potential in the classical Scharfetter-Gummel discretization ansatz. The Poisson equation (55b) and the momentum equation (55c) are discretized using the classical two point flux approximation.

3 Results

In the following we perform different numerical simulations to elaborate the dynamics of the derived model. Different boundary conditions are applied on the inner boundary to implement different experiments. Depending on the application, the system is solved transient or in steady state.

3.1 Calcium-selective ion channel

In order to compare the model with experimental data we assume that the system is in steady state, such that the partial derivative with respect to time in (55a) vanishes. Furthermore, we assume that the process inside the selectivity filter is diffusion dominant, such that the chemical reactions on the interfaces $S^{\text{out,SF}}$ and $S^{\text{in,SF}}$ are fast compared to the diffusion inside Ω^{SF} and can be assumed to be in equilibrium. This leads to continuous ion flow. In the inner and outer bath we consider a mixture of sodium ($A_1 = A_{\text{Na}^+}$), calcium ($A_2 = A_{\text{Ca}^{2+}}$) and chloride ($A_3 = A_{\text{Cl}^-}$) ions, as well as water molecules ($A_0 = A_{\text{H}_2\text{O}}$) as solvent. Within the selectivity filter domain we do not expect water, instead we have the lattice forming species such as oxygen ($A_0 = A_{\text{O}^{-1/2}}$ in Ω^{SF}).

The dimensions of our simulation domain are based on those for calcium selective L-type channels [6, 40, 43] and are given in Figure 6. For all simulations we use a cylindrically symmetric domain with a radius of $r_{\text{domain}} = 25\,\text{Å}$ and a length of $l_{\text{domain}} = 40\,\text{Å}$. The lipid bilayer has a thickness of $d_{\text{lip}} = 20\,\text{Å}$. In the center the membrane contains the pore with a radius of $r = 4.5\,\text{Å}$ at the narrowest point. The selectivity filter region within the channel has a length of $l = 14\,\text{Å}$. We do not apply the surface charge on the whole selectivity filter but rather to a smaller part since the ions mainly interact with the negative charged EEEE (Glu-Glu-Glu-Glu) locus. The length of the applied surface charge is $l_{\text{charge}} = 8\,\text{Å}$.

Note that if the parameter values are not explicitly mentioned in the text, they have been chosen as in the table 2.

3.1.1 Comparison with experimental data

We compare our simulation results to an experimentally measured current by Almers et. al [2]. In their work they studied the calcium selectivity of a single-file pore. They measured the total current through the pore and observed, that the permeability of calcium channels depends on the Ca^{2+} concentration.

To compare the model to the data we calculate the ionic current for a fixed applied membrane potential with (PD-BCs) $\varphi^{\text{out}} = 0\,\text{mV}$ and $\varphi^{\text{in}} = -20\,\text{mV}$, s.t. $E = -20$ mV. On the boundaries S^{out} and S^{in} we use Dirichlet boundary conditions for the ion species (CD-BCs) with bulk concentrations $[\text{NaCl}]_{\text{out}} = [\text{NaCl}]_{\text{in}} = 32\,\text{mM}$, $[\text{CaCl}_2]_{\text{out}} = (5.13 \cdot 10^{-7} - 13.18)\,\text{mM}$ and $[\text{CaCl}_2]_{\text{in}} = 0\,\text{mM}$. For the pressure we apply Dirichlet boundary conditions $p^{\text{out}} = p^{\text{in}} = 0\,\text{Pa}$. Within the selectivity filter a permanent surface charge is applied via (SC-BC) with $q_s^{\text{lip,SF}} = -2\,e_0\,\text{C m}^{-2}$. For the pressure and the ion species we define (NF-BCs). The number of lattice sites is calculated from relation (31) with the assumption that our simulation domain is cylindrical symmetric. We find for $z_{n_\ell} = -1$ and $n_\ell = 2\,\text{mM}$ that $\zeta = 0.13$. However, we assume during the simulations that there is no backbone charge, i.e., $z_{n_\ell} = 0$.

For the cations we derive different diffusion coefficient within the selectivity filter, with $D^{\text{SF}}_{\text{Ca}^{2+}} = 2.5 \cdot 10^{-4} \cdot D^j_{\text{Ca}^{2+}}$ and $D^{\text{SF}}_{\text{Na}^+} = 1.5 \cdot 10^{-3} \cdot D^j_{\text{Na}^+}$, with $j = \{\text{out}, \text{in}\}$. All other relevant parameter values are given in Table 2.

The diffusion coefficients and the number of lattice sites within the selectivity filter domain were determined by fitting the model to the experimental data from Figure 11 in [2]. Figure 7 shows the comparison of the total ionic current (circles) calculated from the simulation compared to the experimentally measured total current (crosses) from Figure 11 in [2]. We find that the model is in agreement with the data. The partial sodium (I_{Na^+}) and calcium ($I_{\text{Ca}^{2+}}$) currents are denoted by the blue and the red lines, respectively. It illustrates that the channel is blocked to monovalent cations at a certain extracellular Ca^{2+} concentration and that the current is then dominated by the Ca^{2+} current. The external calcium

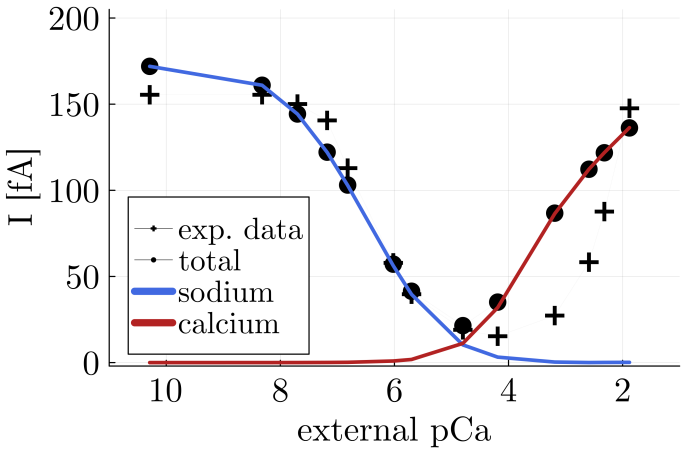

Figure 7: Total current for different calcium concentrations in the outer bath. Model simulation (circles) compared to experimental data (crosses) from Almers et al. [2]. Sodium current (blue) and calcium current (red) for different calcium cocentrations pCa = $-\log_{10}([\mathrm{CaCl_2}]_{\mathrm{out}})$ in the outer bath.

concentration is given in pCa = $-\log_{10}([\mathrm{CaCl_2}]_{\mathrm{out}})$.

3.1.2 Current and the Na^+ and Ca^{2+} permeability of the channel

In the following we show a numerical study, where the influence of different parameters on the current and the Na^+ and Ca^{2+} permeability of the channel was investigated. Figure 8a shows the sodium and calcium currents for different surface charges. It can be found, that for a decreasing surface charge, both $I_{\mathrm{Na^+}}$ and $I_{\mathrm{Ca^{2+}}}$ decrease. This indicates that the current is proportional to the surface charge, i.e., decreasing the surface charge by a factor of $0.8 - 0.9$ leads to an decrease of the current by a factor of $0.8 - 0.9$. In addition a shift towards higher Ca^{2+} concentrations can be observed. The curve of the sodium current is shifted to the right towards higher calcium concentrations. However, this effect needs to be investigated in more detail.

Enhancing the calcium diffusion within the selectivity filter domain by a factor of 1.5 leads to an increase of the peak $I_{\mathrm{Ca^{2+}}}$ by a factor of 1.5. A decrease in the mobility by 0.5 leads to a decrease in the peak calcium current by a factor of 0.5. This indicates that the current is proportional to the diffusion coefficient of calcium within the selectivity filter. Furthermore, as can be seen in Figure 8b, this has no effect on the sodium current.

As shown in Figure 8c also the sodium current is proportional to the diffusion coefficient of sodium. An increase (decrease) in the sodium mobility within the selectivity filter leads to an increase (decrease) in the peak $I_{\mathrm{Na^+}}$ and does not influence the permeation of calcium.

Applying a backbone charge with $z_{n_\ell} = -1$ in addition to the surface charge leads to a left shift of sodium and calcium current towards smaller calcium concentrations. The curves now cross at pCa = 5.5 while when only applying the surface charge they cross at pCa$= 4.8$. This is illustrated in Figure 8d. Setting the surface charge to zero ($q_s^{\mathrm{SF,lip}} = 0$) and applying only the backbone charge of $z_{n_\ell} = -3.7$ (which is equivalent to a surface charge of $q_s^{\mathrm{SF,lip}} = -2e_0$) gives smaller peak currents and also a right shift of sodium current towards higher Ca^{2+} concentrations. Figure 9 shows the calcium (left) and sodium (right) currents plotted as a function of the surface charge within the selectivity filter for different external calcium concentrations. The calcium current increases continuously for an increasing

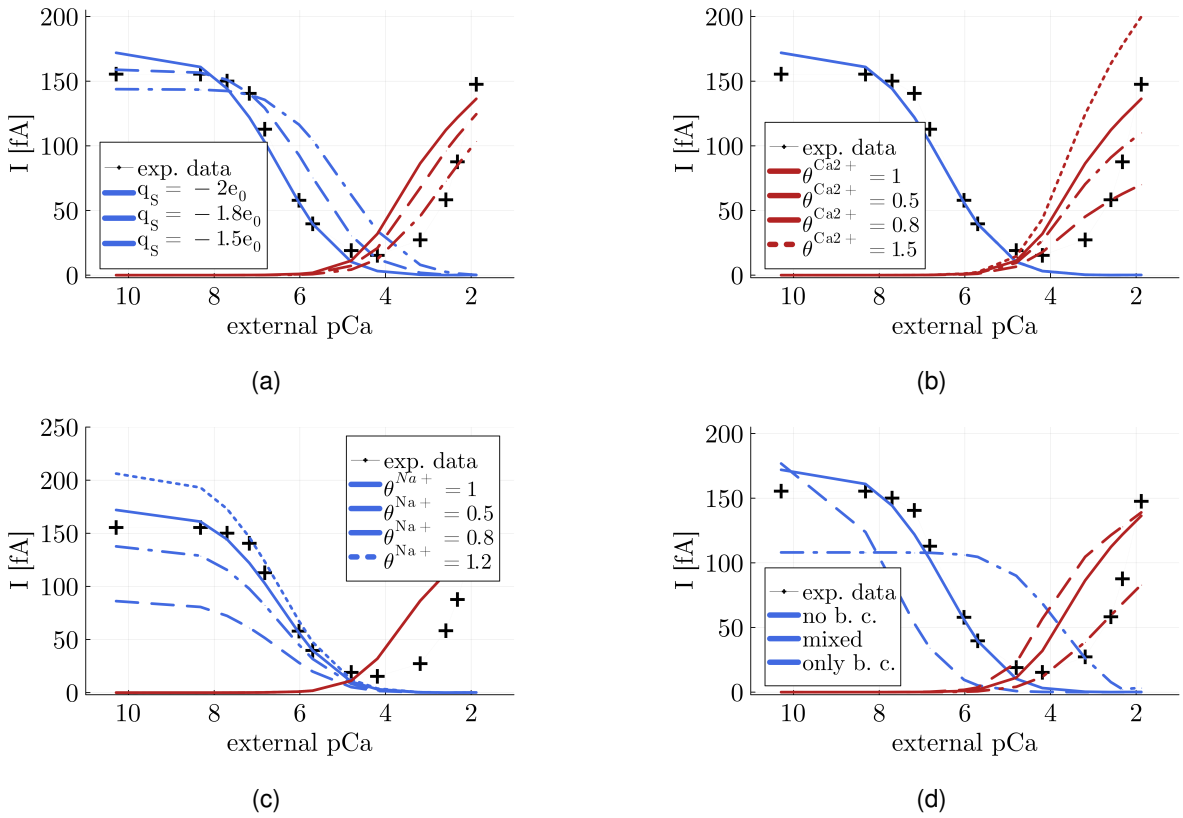

Figure 8: (a) Total current for different channel surface charges with $q_S = q_s^{\text{SF,lip}}$. (b) and (c) Total current for different diffusion coefficients of Ca^{2+} and Na^+ within the selectivity filter domain, respectively. (d) Total current for three cases: only surface charge, only backbone charge (b. c.) and both.

surface charge. The sodium current rises while the surface charge increases but starts to decrease again for $q_s^{\text{SF,lip}} \leq -1.4e_0$. For higher calcium concentrations the sodium current decreases already for smaller surface charges, compared to lower calcium concentrations.

3.2 Step depolarization

In the following we will apply time-dependent boundary conditions for the membrane potential to calculate ion currents for step depolarisation. Therefore we solve the transient system. The simulation was performed from an initial time $t = 0\,\text{s}$ to a final time of $t = 0.3\,\text{s}$. The initial potential was $E = -60\,\text{mV}$ and was switched to $E = -40\,\text{mV}$ $(-20\,\text{mV}, -10\,\text{mV})$ after $0.1\,\text{s}$, with $\varphi^{\text{out}} = 0$, s.t. $\varphi^{\text{in}} = E$. The simulations were carried out for two different external calcium concentrations pCa$= 7.7$ and pCa$= 3.2$. In Figure 10 calcium and sodium currents are plotted over time for pCa$= 7.7$. It can be observed that the currents rise sharply after a potential switch. In the first few seconds after depolarization an outward current is measured until a steady inward current is established. The peak calcium currents are over three orders of magnitude smaller and take approximately $0.1\,\text{s}$ longer to reach steady state. After approximately $0.175\,\text{s}$ the Ca^{2+} current declines. When changing the external calcium concentration to pCa$= 3.2$ the peak sodium currents are still approximately two times higher than the peak calcium currents. In that case the steady state sodium current is reached later then the steady state calcium current. after $0.25\,\text{s}$ the Na^+ current declines. The difference in the peak currents can be explained by the different concentrations of sodium and calcium in the intracellu-

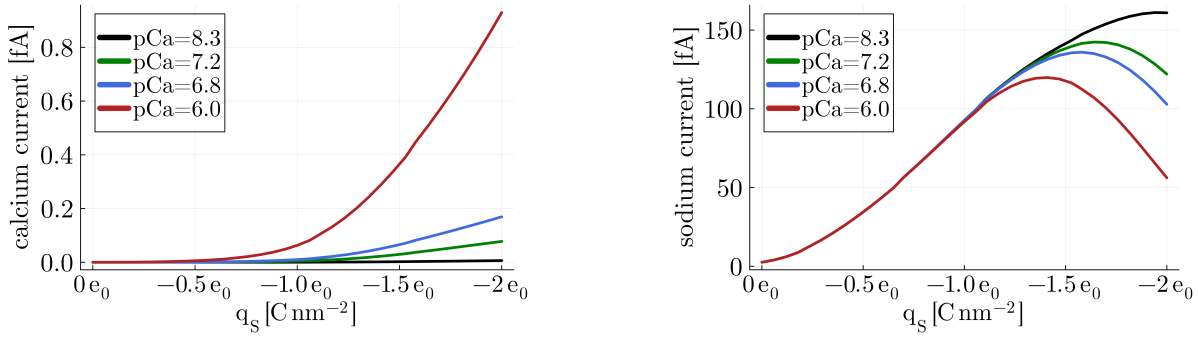

(a) (b)

Figure 9: (a) Calcium current and (b) sodium current as a function of the surface charge inside the selectivity filter for different external calcium concentrations.

lar domain. The initial Ca^{2+} concentration was set to zero, whereas the initial Na^{+} concentration was $32\,\mathrm{mM}$. The magnitudes of the different currents are the same as in the previous experiment.

3.3 Cyclic voltammetry

Similar to the previous section, we apply a time-dependent membrane potential. However, instead of a pulse, the potential is now a waveform, i.e., it increases (decreases) linear in time. The applied potential as a function of time is given by Figure 11a. The current was measured for a calcium concentration in the outer and inner bath of pCa$= 4.8$. For this simulations we chose the calcium concentrations equivalent in the intra- and extracellular. The scanning rate for the potential is $v^{\text{scan}} = 2596.5\,\mathrm{Vs}^{-1}$. The maximum potential is $E = 50\,\mathrm{mV}$ and the minimum potential is $E = -50\,\mathrm{mV}$. We apply one cycle that takes around $t = 75\,\mu\mathrm{s}$. Figure 11b shows the voltammogram for calcium [11, 18]. The scan starts in the direction of negative membrane potentials, resulting in an inward calcium current. As the potential becomes more negative, the current continues to increase until the switching point is reached. After reversing the scanning direction, a smaller inward current is measured, resulting in a separation between the two curves. When a membrane potential of about $6 - 7\,\mathrm{mV}$ is reached, the current changes sign and an outward current is measured. After changing the scanning direction again, the outward current starts to decrease. For positive membrane potentials, the span between the two curves is not as large as for negative potentials. The sodium current shows a similar behavior, with the exception that the current increases after switching the scanning direction (Figure 11c).

3.4 Current-voltage relations

It is possible to calculate current-voltage (IV) relations under different conditions such as different calcium concentrations or different surface charges. The IV-relations for calcium and sodium are given in Figure 12. The currents were calculated for different membrane potentials from $E = -100\,\mathrm{mV}$ to $E = 100\,\mathrm{mV}$. For each membrane potential the system was solved in steady state.

In a first experiment the IV-relation was calculated for different Ca^{2+} concentrations in the outer and inner bath, namely pCa$= 5.7$, pCa$= 4.8$ and pCa$= 4.2$. As expected the calcium current increases (Figure 12a) for higher Ca^{2+} concentrations while the sodium current decreases (Figure 12b). In a second experiment the surface charge was varied. In that scenario the IV-relation was measured for

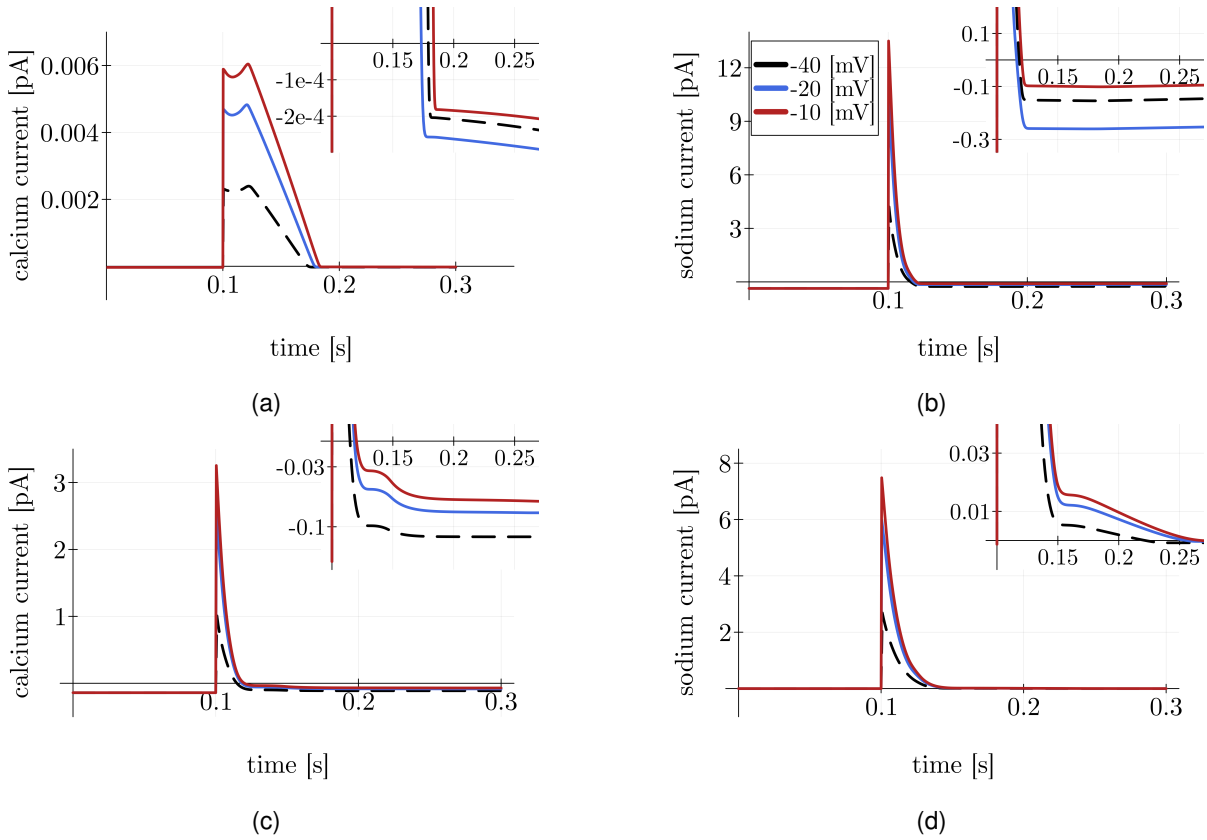

Figure 10: (a) Calcium current and (b) sodium current as a function of time for different step depolarizations $E = -40\,\text{mV}$, $E = -20\,\text{mV}$ and $E = -00\,\text{mV}$ and an external calcium concentration of pCa$= 7.7$. (c) Calcium current and (d) sodium current for an external calcium concentration of pCa$= 3.2$.

pCa$= 4.8$ in the inner and outer domain and for $q_s^{\text{SF,lip}} = q_S = -1.5e_0$, $q_S = -1.7e_0$ and $q_S = -2e_0$. As the surface charge increases also the calcium current increases (Figure 12c). However, the sodium current decreases with increasing surface charge (Figure 12d). This coincides with the result from section 3.1.2.

It is noteworthy that the currents change sign at a potential of around $E = 6 - 7\,\text{mV}$. If the surface charge is reduced, the sign change shifts in the direction of the origin, i.e. at $q_S = 0$ the currents would change sign at a membrane potential of $E = 0\,\text{mV}$.

4 Discussion and outlook

This work focuses on the mathematical consistent modelling of the selectivity filter. Our approach is to include the selectivity filter as an additional embedded domain and treat it as a polymeric or solid electrolyte. The assumption is that the filter region is formed by immobile scaffold forming species that mix and interact with the channel passing ions.

In previous modeling approaches, the structural charges of the selectivity filter were included by introducing confined oxygen ions. These ions were assumed to move freely within the selectivity filter but not to enter the two baths. The confinement was modeled by a hard-wall potential [27, 39, 43]. Different approaches, such as DFT [25, 27] or MSA [38], were used to derive the chemical potential

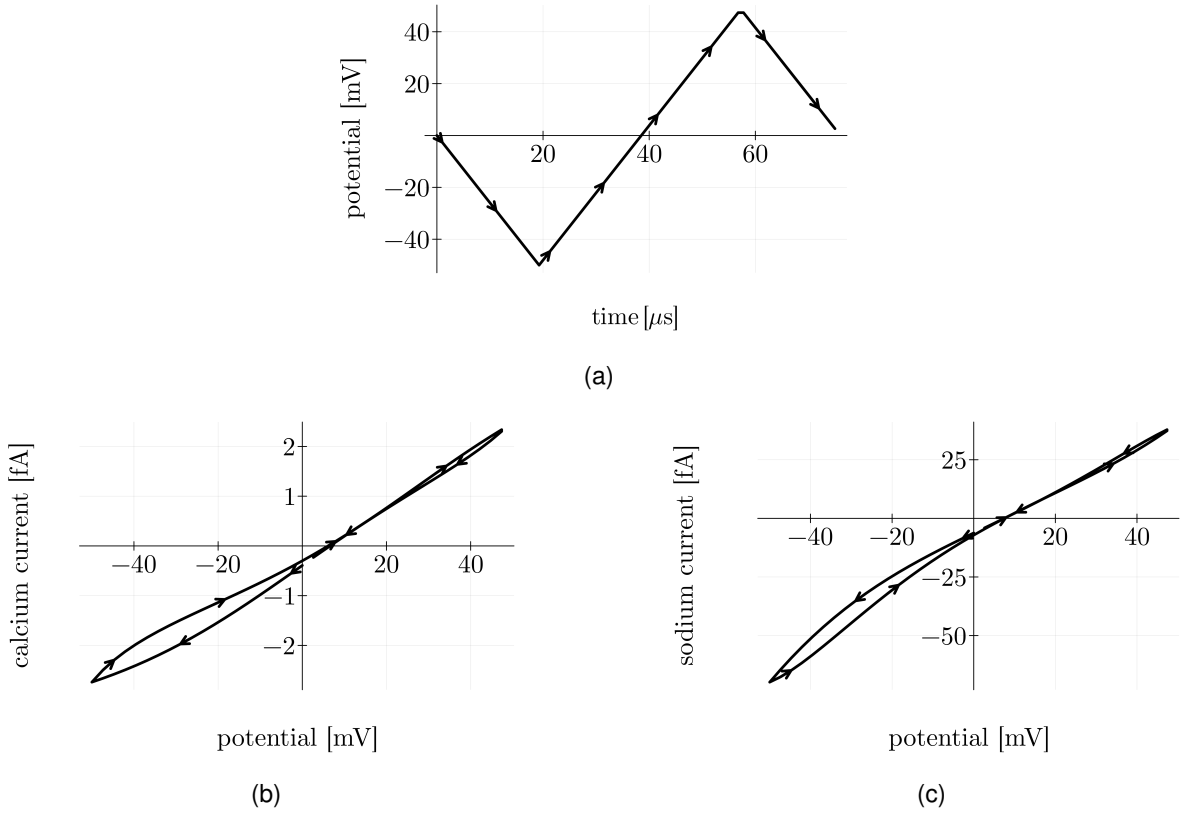

Figure 11: (a) Membrane potential as a function of time for one cycle. (b) Voltammogramm for calcium. (c) Voltammogram for sodium.

for the species within the selectivity filter and the binding selectivity. Solvation effects are described implicitly by different dielectric properties within the different phases [26, 43]. Therefore, the dielectric constant is often treated as a function of space [32]. In addition, the different mobilities of the ions within the selectivity filter are modeled with location-dependent diffusion coefficients, which are also described as continuously differentiable functions of space [27, 40]. Liu and Eisenberg [39, 41] developed a model were they treated the free moving oxygen ions as multiple additional binding domains. Algebraic equations must therefore be solved to calculate the electrostatic potential and the steric potential within these domains. The resulting electrostatic potential is then coupled with the PNPB system through a Dirichlet boundary condition. The underlying idea is that within the selectivity filter region multiple binding sites exists and that the permeating ions hop from one site to the other [26].

We account for binding sites and the hoping of ions by assuming that the immobile species form lattice sites on which channel passing species can move, i.e., ions can thus only move from one lattice site to another. This idea is incorporated in the model within the free energy density by the mixing entropy. Furthermore, we take into account solvation and desolvation effects within the free energy density of the system and by chemical reactions on interfaces. Treating the selectivity filter as a separate region allows a consistent derivation of different chemical potential functions within different phases for the species based on non-equilibrium thermodynamics. Charges of the protein are incorporated by a backbone charge and by surface charges.

A first numerical example illustrates that the model is able to fit experimental results. It reproduces the measured total current in a calcium channel for varying Ca^{2+} concentrations in the extracellular bath. The simulations show, that for low calcium concentrations the channel is conductive for sodium.

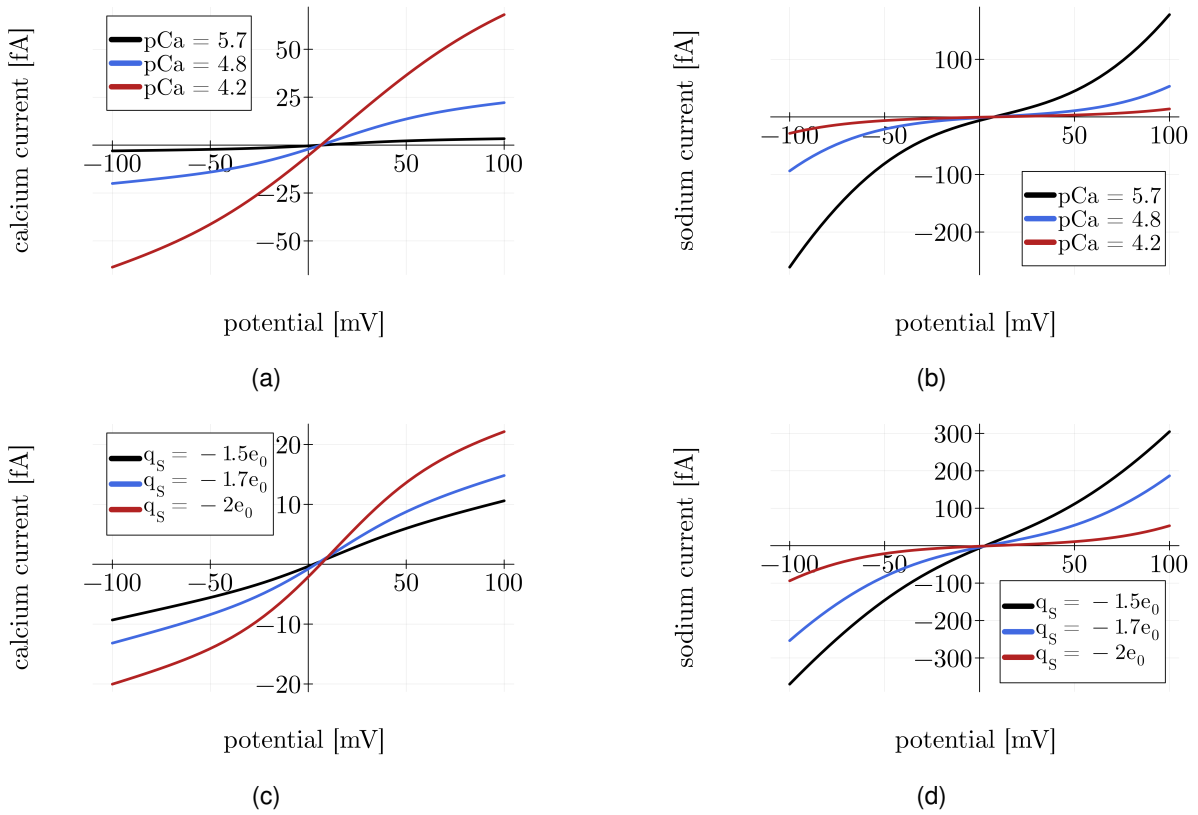

Figure 12: (a) Current voltage relation for calcium current and (b) sodium current for different external calcium concentrations. (c) Current voltage relation for calcium and (d) for sodium for different surface charges within the selectivity filter.

However, the determined diffusion coefficients within the selectivity filter are around one order of magnitude smaller than those proposed by MD simulations and other continuum models. Here, diffusion coefficients were determined that are 5-10 times smaller than in the bulk [1, 28, 40, 42, 51]. Nevertheless, one has to be careful when comparing these results, for example, Allen et al. [1] study KcsA potassium channels with a length of 40 Å while our channel has a lenght of 20 Å . Mamonov et al. study the diffusion of K^+ in Gramacidin A channel and vary the dielectric constant within the selectivity filter, while we keep the dielectric properties constant throughout the whole domain.

The parameter study depicts that mobility and electrostatic forces do influence the ion current. Furthermore, we find that the current is proportional to the diffusion coefficients and the surface charge within the channel. The investigation of the currents as a function of the surface charge shows that the selectivity between divalent calcium and monovalent sodium ions depends on the electric field within the selectivity filter. This is consistent with the statement that the selectivity depends on both finite volume effects and on the electrostatic forces [5, 43]. Another example of calcium selective ion channels are ryanodine receptors (RyRs). Wei et al. [53] and Gillespie et al. [28] found that the selectivity in RyR1, for example, also depends mainly on the electric field formed by the negatively charged residues rather than on the desolvation of the ions or other physical phenomena.

Other proposed models provide similar qualitative results as our model. Nevertheless, our approach provides a consistent description of the selectivity filter within the continuum formulation without the need to solve additional equations. This allows for a straightforward numerical implementation of the system. Furthermore, many models do not explicitly take dehydration of ions into account when they

enter the selectivity filter. Throughout the simulations we assumed that interface reactions are fast compared to the diffusion such that the ion flow is continuous. In a future study we want to include interface reactions and investigate their influence on ion flux and selectivity of the channel. The selectivity of nanopores also plays an important role in technological applications such as water treatment and desalination [19]. Here, the knowledge of biological ion channels is used to design artificial pores. It has been shown that the following characteristics have an influence on selectivity: dielectric exclusion, pore length, pore size, and the binding sites [19]. These are further aspects that could be taken into account in a parameter study by varying the dielectric constant in the channel, changing the length of the selectivity filter, varying length and position of the surface charge, or by changing the diameter of the pore.

The presented model framework allows the study of ion movement through nanopores under different conditions such as different channel properties and bulk concentrations. It enables to easily change constituents within the electrolyte and it is possible to include backbone and surface charges within the channel or on the lipid bilayer. Furthermore, different chemical properties of the ions can be taken into account by including different chemical potentials. Through a consistent coupling of diffusion and the incompressibility of the electrolyte it is possible to include ions of different sizes in the model. Our model provides a tool for the analytical and numerical investigation of parameter dependencies. By applying different types of boundary conditions a variety of different numerical experiments can be performed.

Acknowledgements. The authors thank Bob Eisenberg (Rush University) for fruitful discussions.

References

[1] Toby W Allen, Serdar Kuyucak, and Shin-Ho Chung. Molecular dynamics estimates of ion diffusion in model hydrophobic and kcsa potassium channels. *Biophysical Chemistry*, 86(1):1–14, July 2000.

[2] W Almers and E W McCleskey. Non-selective conductance in calcium channels of frog muscle: calcium selectivity in a single-file pore. *The Journal of Physiology*, 353(1):585–608, aug 1984.

[3] W Almers, E W McCleskey, and P T Palade. A non-selective cation conductance in frog muscle membrane blocked by micromolar external calcium ions. *The Journal of Physiology*, 353(1):565–583, aug 1984.

[4] L. Blum. Mean spherical model for asymmetric electrolytes: I. method of solution. *Molecular Physics*, 30(5):1529–1535, November 1975.

[5] Dezsö Boda, David D. Busath, Douglas Henderson, and Stefan Sokołowski. Monte carlo simulations of the mechanism for channel selectivity: the competition between volume exclusion and charge neutrality. *The Journal of Physical Chemistry B*, 104(37):8903–8910, aug 2000.

[6] Dezső Boda, Mónika Valiskó, Douglas Henderson, Bob Eisenberg, Dirk Gillespie, and Wolfgang Nonner. Ionic selectivity in l-type calcium channels by electrostatics and hard-core repulsion. *Journal of General Physiology*, 133(5):497–509, April 2009.

[7] Dieter Bothe and Pierre Étienne Druet. On the structure of continuum thermodynamical diffusion fluxes—a novel closure scheme and its relation to the maxwell–stefan and the fick–onsager approach. *International Journal of Engineering Science*, 184:103818, 2023.

[8] M Burger, B Schlake, and M-T Wolfram. Nonlinear poisson–nernst–planck equations for ion flux through confined geometries. *Nonlinearity*, 25(4):961–990, mar 2012.

[9] W. A. Catterall. Voltage-gated calcium channels. *Cold Spring Harbor Perspectives in Biology*, 3(8):a003947–a003947, jul 2011.

[10] William A. Catterall. Excitation-contraction coupling in vertebrate skeletal muscle: A tale of two calcium channels. *Cell*, 64(5):871–874, mar 1991.

[11] Richard Guy Compton and Craig E Banks. *Understanding voltammetry*. World Scientific, 2018.

[12] S.R. De Groot and P. Mazur. *Non-Equilibrium Thermodynamics*. Dover Books on Physics. Dover Publications, 2013.

[13] Lucie Delemotte, Werner Treptow, Michael L. Klein, and Mounir Tarek. Effect of sensor domain mutations on the properties of voltage-gated ion channels: Molecular dynamics studies of the potassium channel kv1.2. *Biophysical Journal*, 99(9):L72–L74, nov 2010.

[14] Declan A. Doyle, Joao Morais Cabral, Richard A. Pfuetzner, Anling Kuo, Jacqueline M. Gulbis, Steven L. Cohen, Brian T. Chait, and Roderick MacKinnon. The structure of the potassium channel: Molecular basis of K^+ conduction and selectivity. *Science*, 280(5360):69–77, apr 1998.

[15] W. Dreyer, C. Guhlke, and M. Landstorfer. A mixture theory of electrolytes containing solvation effects. *Electrochemistry Communications*, 43:75–78, jun 2014.

[16] Wolfgang Dreyer, Clemens Guhlke, and Rüdiger Müller. Overcoming the shortcomings of the nernst–planck model. *Physical Chemistry Chemical Physics*, 15(19):7075, 2013.

[17] Wolfgang Dreyer, Clemens Guhlke, and Rüdiger Müller. Bulk-surface electrothermodynamics and applications to electrochemistry. *Entropy*, 20(12):939, dec 2018.

[18] Noémie Elgrishi, Kelley J. Rountree, Brian D. McCarthy, Eric S. Rountree, Thomas T. Eisenhart, and Jillian L. Dempsey. A practical beginner's guide to cyclic voltammetry. *Journal of Chemical Education*, 95(2):197–206, November 2017.

[19] Razi Epsztein, Ryan M. DuChanois, Cody L. Ritt, Aleksandr Noy, and Menachem Elimelech. Towards single-species selectivity of membranes with subnanometre pores. *Nature Nanotechnology*, 15(6):426–436, June 2020.

[20] Steven W. Flavell and Michael E. Greenberg. Signaling mechanisms linking neuronal activity to gene expression and plasticity of the nervous system. *Annual Review of Neuroscience*, 31(1):563–590, jul 2008.

[21] Emelie Flood, Céline Boiteux, Bogdan Lev, Igor Vorobyov, and Toby W. Allen. Atomistic simulations of membrane ion channel conduction, gating, and modulation. *Chemical Reviews*, 119(13):7737–7832, jun 2019.

[22] J. Fuhrmann. Comparison and numerical treatment of generalised Nernst–Planck models. *Computer Physics Communications*, 196:166–178, 2015.

[23] Jürgen Fuhrmann and Contributors. Voronoifvm.jl: Finite volume solver for coupled nonlinear partial differential equations, 2022. URL: https://doi.org/10.5281/ZENODO.3529808.

[24] Benoît Gaudeul and Jürgen Fuhrmann. Entropy and convergence analysis for two finite volume schemes for a nernst–planck–poisson system with ion volume constraints. *Numerische Mathematik*, 151(1):99–149, apr 2022.

[25] Dirk Gillespie. Energetics of divalent selectivity in a calcium channel: the ryanodine receptor case study. *Biophysical journal*, 94:1169–1184, February 2008.

[26] Dirk Gillespie and Dezsö Boda. The anomalous mole fraction effect in calcium channels: A measure of preferential selectivity. *Biophysical Journal*, 95(6):2658–2672, sep 2008.

[27] Dirk Gillespie, Wolfgang Nonner, and Robert S Eisenberg. Coupling poisson nernst planck and density functional theory to calculate ion flux. *Journal of Physics: Condensed Matter*, 14(46):12129–12145, nov 2002.

[28] Dirk Gillespie, Le Xu, Ying Wang, and Gerhard Meissner. (de)constructing the ryanodine receptor: modeling ion permeation and selectivity of the calcium release channel. *The Journal of Physical Chemistry B*, 109(32):15598–15610, jul 2005.

[29] H.K. Gummel. A self-consistent iterative scheme for one-dimensional steady state transistor calculations. *IEEE Transactions on Electron Devices*, 11(10):455–465, October 1964.

[30] Thomas Hof, Sébastien Chaigne, Alice Récalde, Laurent Sallé, Fabien Brette, and Romain Guinamard. Transient receptor potential channels in cardiac health and disease. *Nature Reviews Cardiology*, 16(6):344–360, jan 2019.

[31] Scott A. Hollingsworth and Ron O. Dror. Molecular dynamics simulation for all. *Neuron*, 99(6):1129–1143, sep 2018.

[32] T. L. Horng, R. S. Chen, M. V. Leonardi, F. Franciolini, and L. Catacuzzeno. A multi-scale approach to model K^+ permeation through the KcsA channel. *Frontiers in Molecular Biosciences*, 9, jul 2022.

[33] Leighton T. Izu, Peter Kohl, Penelope A. Boyden, Masahito Miura, Tamas Banyasz, Nipavan Chiamvimonvat, Natalia Trayanova, Donald M. Bers, and Ye Chen-Izu. Mechano-electric and mechano-chemo-transduction in cardiomyocytes. *The Journal of physiology*, 598:1285–1305, April 2020.

[34] M. Landstorfer. On the dissociation degree of ionic solutions considering solvation effects. *Electrochemistry Communications*, 92:56–59, jul 2018.

[35] M. Landstorfer, C. Guhlke, and W. Dreyer. Theory and structure of the metal-electrolyte interface incorporating adsorption and solvation effects. *Electrochimica Acta*, 201:187–219, may 2016.

[36] M. Landstorfer and R. Müller. Thermodynamic models for a concentration and electric field dependent susceptibility in liquid electrolytes. *Electrochimica Acta*, 428:140368, oct 2022.

[37] Manuel Landstorfer. Boundary conditions for electrochemical interfaces. *Journal of The Electrochemical Society*, 164(11):E3671–E3685, 2017.

[38] Jinn-Liang Liu and Bob Eisenberg. Correlated ions in a calcium channel model: A poisson–fermi theory. *The Journal of Physical Chemistry B*, 117(40):12051–12058, sep 2013.

[39] Jinn-Liang Liu and Bob Eisenberg. Poisson-nernst-planck-fermi theory for modeling biological ion channels. *The Journal of Chemical Physics*, 141(22):22D532, dec 2014.

[40] Jinn-Liang Liu and Bob Eisenberg. Numerical methods for a poisson-nernst-planck-fermi model of biological ion channels. *Physical Review E*, 92(1):012711, jul 2015.

[41] Jinn-Liang Liu and Bob Eisenberg. Molecular mean-field theory of ionic solutions: A poisson-nernst-planck-bikerman model. *Entropy*, 22(5):550, may 2020.

[42] Artem B. Mamonov, Rob D. Coalson, Abraham Nitzan, and Maria G. Kurnikova. The role of the dielectric barrier in narrow biological channels: A novel composite approach to modeling single-channel currents. *Biophysical Journal*, 84(6):3646–3661, June 2003.

[43] Wolfgang Nonner, Luigi Catacuzzeno, and Bob Eisenberg. Binding and selectivity in l-type calcium channels:a mean spherical approximation. *Biophysical Journal*, 79(4):1976–1992, oct 2000.

[44] Tamara Rosenbaum, Miguel Benítez-Angeles, Raúl Sánchez-Hernández, Sara Luz Morales-Lázaro, Marcia Hiriart, Luis Eduardo Morales-Buenrostro, and Francisco Torres-Quiroz. TRPV4: A physio and pathophysiologically significant ion channel. *International Journal of Molecular Sciences*, 21(11):3837, may 2020.

[45] Roland Roth and Dirk Gillespie. Shells of charge: a density functional theory for charged hard spheres. *Journal of Physics: Condensed Matter*, 28(24):244006, April 2016.

[46] Benoît Roux. Ion channels and ion selectivity. *Essays in Biochemistry*, 61(2):201–209, may 2017.

[47] Benoît Roux, Simon Bernèche, Bernhard Egwolf, Bogdan Lev, Sergei Y. Noskov, Christopher N. Rowley, and Haibo Yu. Ion selectivity in channels and transporters. *Journal of General Physiology*, 137(5):415–426, apr 2011.

[48] D.L. Scharfetter and H.K. Gummel. Large-signal analysis of a silicon read diode oscillator. *IEEE Transactions on Electron Devices*, 16(1):64–77, January 1969.

[49] Z. Schuss, B. Nadler, and R. S. Eisenberg. Derivation of poisson and nernst-planck equations in a bath and channel from a molecular model. *Physical Review E*, 64(3):036116, aug 2001.

[50] J. Shewchuk. Triangle: A two-dimensional quality mesh generator and Delaunay triangulator. URL: http://www.cs.cmu.edu/q̃uake/triangle.html. Accessed 2023-12-01.

[51] G.R. Smith and M.S.P. Sansom. Dynamic properties of na+ ions in models of ion channels: A molecular dynamics study. *Biophysical Journal*, 75(6):2767–2782, December 1998.

[52] Paulina Stokłosa, Anna Borgström, Sven Kappel, and Christine Peinelt. TRP channels in digestive tract cancers. *International Journal of Molecular Sciences*, 21(5):1877, mar 2020.

[53] Risheng Wei, Xue Wang, Yan Zhang, Saptarshi Mukherjee, Lei Zhang, Qiang Chen, Xinrui Huang, Shan Jing, Congcong Liu, Shuang Li, Guangyu Wang, Yaofang Xu, Sujie Zhu, Alan J Williams, Fei Sun, and Chang-Cheng Yin. Structural insights into Ca^{2+}-activated long-range allosteric channel gating of RyR1. *Cell Research*, 26(9):977–994, aug 2016.

[54] Yufeng Zhou, Joao H. Morais-Cabral, Amelia Kaufman, and Roderick MacKinnon. Chemistry of ion coordination and hydration revealed by a k+ channel-fab complex at 2.0 å resolution. 414(6859):43–48, nov 2001.

A Parameter values used to simulate an calcium-selective ion channel

Symbol	Meaning	Value	Unit
T	temperature	298.15	K
e_0	elementary charge	1.602×10^{-19}	C
k_B	Boltzman constant	1.380×10^{-23}	J K^{-1}
N_A	Avogadro constant	6.022×10^{23}	mol^{-1}
$F = e_0 N_A$	Faraday constant	9.648×10^{4}	C mol^{-1}
$R = k_B N_A$	Gas constant	8.314	J mol^{-1} K^{-1}
ε_0	vacuum permittivity	8.854×10^{-12}	F m^{-1}
$\chi = \varepsilon_r - 1$	dielectric susceptibility	86.9	-
ε_r	relativ permittivity water	87.9	-
$D^j_{Ca^{2+}}$, $D^j_{Na^+}$, $D^j_{Cl^-}$	diffusion coefficients	$[0.79, 1.334, 2.032] \times 10^{-9}$	m^2 s^{-1}
$D^{SF}_{Ca^{2+}}$, $D^{SF}_{Na^+}$ in Ω^{SF}	diffusion coefficients	$[0.25D^j_{Ca^{2+}}, 1.5D^j_{Na^+}] \times 10^{-3}$	m^2 s^{-1}
z_{H_2O}, $z_{Ca^{2+}}$, z_{Na^+}, z_{Cl^-}	charge number of ions	0, 2, 1, -1	-
M_{H_2O}, $M_{Ca^{2+}}$, M_{Na^+}, M_{Cl^-}	molar weights	18.0, 40.1, 23.0, 35.5	g mol^{-1}
v_{H_2O}, $v_{Ca^{2+}}$, v_{Na^+}, v_{Cl^-}	molar volumes	[55.4, 26.20, 23.78, 17.39]$\times10^{-6}$	m^3 mol^{-1}
$q^{SF,lip}_s = q_S$	charge channel wall	$-2e_0$	C nm^{-2}
$q^{out,lip}_s$, $q^{in,lip}_s$	charge lipid bilayer	0	C nm^{-2}
$[CaCl_2]_{in}$, $[CaCl_2]_{out}$	bulk concentrations	0, 10	mM
$[NaCl]_{in}$, $[NaCl]_{out}$	bulk concentrations	32, 32	mM
φ^{in}, φ^{out}	bulk potential	-20, 0	mV
$\kappa_{Ca^{2+}}$, κ_{Na^+}, κ_{Cl^-}	solvation numbers	30, 60, 30	-
r	channel radius	4.5	Å
l	length of Ω^{SF}	14	Å
l_{charge}	length of $S^{SF,lip}$	8	Å
n_ℓ	scaffold forming species	2	mol L^{-1}

Table 2: Parameter values used to simulate an calcium-selective ion channel.